Science Translational Medicine
AAAS

Dual Inactivation of Akt and ERK by TIC10 Signals Foxo3a Nuclear Translocation, TRAIL Gene Induction, and Potent Antitumor Effects

Joshua E. Allen *et al.*

Sci Transl Med **5**, 171ra17 (2013);
DOI: 10.1126/scitranslmed.3004828

Editor's Summary

TIC'ing Up the TRAIL

TRAIL is a naturally occurring tumor suppressor: It stimulates cell death pathways in a variety of human cancers and thus has been a popular target for the development of anticancer drugs. Previous TRAIL-targeting strategies include synthesis of the recombinant protein and stimulatory antibodies. All of these agents exhibit some of the typical drawbacks of protein-based therapeutics, such as short half-lives and a need to administer the drugs directly into the bloodstream or even into the tumor. Now, Allen and colleagues have discovered a drug, TIC10, which can stimulate production of TRAIL while avoiding the shortcomings of protein-based therapies.

The authors demonstrated that TIC10 can increase TRAIL and stimulate the death of multiple types of human cancer cells both in culture and in mice. The drug was equally effective when given orally or intravenously and effectively penetrated the blood-brain barrier to target glioblastoma, a difficult-to-treat brain tumor. Whereas recombinant TRAIL displayed a short half-life of ~30 min, TIC10 activity persisted in the mice for days, allowing for once-a-week dosing. Toxicity analysis in mice showed no detectable adverse effects from treatment with TIC10. The authors also showed that TIC10 boosts TRAIL function through inactivation of the Akt and MEK signaling proteins, which results in translocation of the transcription factor Foxo3a into the cell nucleus, where it stimulates TRAIL gene expression.

Before TIC10 can be used to treat patients, the drug will need to be tested in clinical trials to confirm safety and efficacy results from mouse studies. In addition, further work is needed to determine the mechanism by which TIC10 causes the dephosphorylation and resulting inactivation of Akt and MEK. However, the discovery of TIC10 clears a path to versatile TRAIL-based cancer therapies.

Science Translational Medicine (print ISSN 1946-6234; online ISSN 1946-6242) is published weekly, except the last week in December, by the American Association for the Advancement of Science, 1200 New York Avenue NW, Washington, DC 20005.

CANCER

Dual Inactivation of Akt and ERK by TIC10 Signals Foxo3a Nuclear Translocation, TRAIL Gene Induction, and Potent Antitumor Effects

Joshua E. Allen,[1,2,3] Gabriel Krigsfeld,[3] Patrick A. Mayes,[3] Luv Patel,[3] David T. Dicker,[1,3] Akshal S. Patel,[1,4] Nathan G. Dolloff,[1,3] Evangelos Messaris,[5] Kimberly A. Scata,[1,3] Wenge Wang,[1] Jun-Ying Zhou,[6] Gen Sheng Wu,[6] Wafik S. El-Deiry[1,2,3,7]*

Recombinant tumor necrosis factor–related apoptosis-inducing ligand (TRAIL) is an antitumor protein that is in clinical trials as a potential anticancer therapy but suffers from drug properties that may limit efficacy such as short serum half-life, stability, cost, and biodistribution, particularly with respect to the brain. To overcome such limitations, we identified TRAIL-inducing compound 10 (TIC10), a potent, orally active, and stable small molecule that transcriptionally induces TRAIL in a p53-independent manner and crosses the blood-brain barrier. TIC10 induces a sustained up-regulation of TRAIL in tumors and normal cells that may contribute to the demonstrable antitumor activity of TIC10. TIC10 inactivates kinases Akt and extracellular signal–regulated kinase (ERK), leading to the translocation of Foxo3a into the nucleus, where it binds to the TRAIL promoter to up-regulate gene transcription. TIC10 is an efficacious antitumor therapeutic agent that acts on tumor cells and their microenvironment to enhance the concentrations of the endogenous tumor suppressor TRAIL.

INTRODUCTION

Tumor necrosis factor–related apoptosis-inducing ligand (TRAIL) is a powerful inducer of apoptosis in a wide range of human cancer cell lines via proapoptotic death receptor 4 (DR4; TRAIL-R1) (*1*) and death receptor 5 (DR5; TRAIL-R2) (*2*, *3*) at the cell surface through engagement of the extrinsic or intrinsic apoptotic pathways (*4*). TRAIL serves as a tumor suppressor during immune surveillance, but this antitumor mechanism is lost during cancer progression. The ability of TRAIL to initiate apoptosis selectively in cancer cells has led to ongoing clinical trials with recombinant TRAIL and the longer-lived TRAIL receptor agonist antibodies, which target either of TRAIL's two proapoptotic death receptors (*5*–*11*). Variants of recombinant TRAIL and other protein-based therapeutics continue to be developed to recapitulate the antitumor efficacy of endogenous TRAIL and to improve its stability (*12*, *13*). Mesenchymal stem cells overexpressing TRAIL have recently been explored to improve the biodistribution of TRAIL to allow for its use in glioma (*14*).

Although current TRAIL-based therapies are costly to produce for clinical applications and may be limited by stability and/or biodistribution, endogenous TRAIL is a robust and selective tumor suppressor and naturally lends itself as a drug target to restore antitumor immunity. We hypothesized that up-regulation of TRAIL expression by a small molecule would lead to potent antitumor effects and improve the biodistribution and pharmacokinetic properties of TRAIL by increasing its half-life as well as its concentration within the tumor microenvironment.

The transcription factors p53 (*15*) and Foxo3a (*16*), which typically serve as tumor suppressors (*17*), positively regulate the TRAIL gene. In our search for TRAIL-inducing compounds that up-regulate the TRAIL gene, we explicitly selected those that do not rely on p53 because p53 is frequently inactivated in late-stage cancers, which causes resistance to many standard-of-care therapies such as 5-fluorouracil and doxorubicin (*18*). Among FOXO family members, Foxo3a transcriptionally regulates the TRAIL gene through a region of the promoter that is downstream of the p53 regulatory site that we previously identified (*15*). Foxo3a is primarily regulated by control of its localization through phosphorylation events that dock the transcription factor to cytoplasmic 14-3-3 proteins and inactivate it (*19*). This phosphorylation is carried out by a number of kinases involved in prosurvival signaling, such as IκB kinase (IKK), serum- and glucocorticoid-induced kinase (SGK), Akt, and extracellular signal–regulated kinase (ERK) (*19*, *20*). In summary, Foxo3a is normally sequestered in the cytoplasm by growth factor/prosurvival signaling pathways, which prevents its ability to activate the TRAIL gene. Thus, modulation of Foxo3a by targeting upstream prosurvival signaling pathways that have well-established roles and are highly conserved in cancer could allow therapeutic up-regulation of the TRAIL gene.

RESULTS

TIC10 stimulates tumor cell production of TRAIL

To overcome limitations of recombinant TRAIL, we screened the National Cancer Institute (NCI) Diversity Set II for small molecules capable of up-regulating endogenous TRAIL gene transcription to pharmacologically increase tumor and host TRAIL protein production. A cell-based bioluminescence reporter screen conducted in TRAIL-resistant

[1]Laboratory of Translational Oncology and Experimental Cancer Therapeutics, Department of Medicine (Hematology/Oncology), Penn State Hershey Cancer Institute, Hershey, PA 17033, USA. [2]Biochemistry and Molecular Biophysics Graduate Group, University of Pennsylvania School of Medicine, Philadelphia, PA 19104, USA. [3]Laboratory of Molecular Oncology and Cell Cycle Regulation, Departments of Medicine, Genetics, and Pharmacology, University of Pennsylvania School of Medicine, Philadelphia, PA 19104, USA. [4]Department of Neurological Surgery, Penn State Hershey Medical Center, Hershey, PA 17033, USA. [5]Department of Surgery, Penn State College of Medicine, Hershey, PA 17033, USA. [6]Program in Molecular Biology and Genetics, Karmanos Cancer Institute, Department of Pathology, Wayne State University School of Medicine, Detroit, MI 48201, USA. [7]American Cancer Society, Atlanta, GA 30329, USA.
*To whom correspondence should be addressed. E-mail: wafik.eldeiry@gmail.com

Bax-null HCT116 human colon cancer cells harboring a TRAIL gene promoter luciferase reporter yielded the small-molecule TIC10 as a TRAIL-inducing compound (Fig. 1A and fig. S1). TIC10 caused a dose-dependent increase in TRAIL mRNA (Fig. 1B) and induced TRAIL protein localization on the cell surface of several cancer cell lines in a p53-independent manner (Fig. 1C). A time-course analysis found that TRAIL was localized to the cell surface as a late event but that this induction could be sustained even after removal of TIC10 from the media (Fig. 1, D and E). Thus. TIC10 exposure led to a significant ($P < 0.05$) and sustained presence of TRAIL on the cell surface of cancer cells.

TIC10 induces TRAIL-mediated apoptosis

TIC10 had broad-spectrum activity against multiple malignancies in vitro (fig. S2A) and induced an increase in sub-G_1 DNA content suggestive of cell death in TRAIL-sensitive HCT116 $p53^{-/-}$ cells, but did not alter the cell cycle profiles of normal fibroblasts at equivalent doses (Fig. 2A). Similarly, TIC10 decreased the clonogenic survival of cancer cell lines and spared normal fibroblasts (Fig. 2, B and D). We also found that TIC10 increased the percentage of sub-G_1 DNA in cancer cells in a p53-independent and Bax-dependent manner, as we previously reported for TRAIL-mediated apoptosis (*21*) (Fig. 2E). As expected for apoptotic cell death, TIC10 activated caspase-3 (Fig. 2F) and increased sub-G_1 DNA content; this effect was significantly ($P < 0.05$) inhibited by co-incubation with the pan-caspase apoptosis inhibitor benzyloxycarbonyl-Val-Ala-Asp-fluoromethylketone (zVAD-fmk) (Fig. 2G). TIC10-induced apoptosis appeared to be specifically mediated by TRAIL, as indicated by inhibition of TIC10-induced cytotoxicity after stable knockdown of TRAIL by short hairpin RNA (shRNA) (Fig. 2H and fig. S2B). Additional evidence for the requirement of TRAIL in TIC10-induced tumor cell death was observed after disruption of the DR5 death domain that modulates proapoptotic TRAIL signaling (Fig. 2I) and through experimental sequestration of TRAIL by use of a blocking antibody (fig. S2C). We also tested the activity of TIC10 on freshly resected colon tumor cells (a mucinous adenocarcinoma resected from an 85-year-old female patient) and found that TIC10 induced TRAIL and had potent cytotoxic effects, unlike 5-fluorouracil (fig. S2, D and E). In addition, we found that the cytotoxic activity of TIC10 was thermally stable, unlike that of TRAIL (Fig. 2J), supporting our central hypothesis. Together, these data demonstrate that TRAIL and TRAIL signaling play a critical role in TIC10-mediated apoptosis.

TIC10 is a TRAIL-dependent antitumor agent in vivo

We found that TIC10 and TRAIL treatment caused tumor regression in the HCT116 $p53^{-/-}$ xenograft to a comparable extent when both are administered as multiple doses (Fig. 3A). Single-dose experiments in HCT116 wild-type (Fig. 3B) and RKO (Fig. 3C) human colon cancer xenograft–bearing mice corroborated the antitumor activity of TIC10. TIC10 also induced regression of MDA-MB-231 human triple-negative breast cancer xenografts, whereas TRAIL-treated tumors progressed; the effect of TIC10 was significantly ($P < 0.005$) inhibited by stable knockdown of TRAIL (Fig. 3D and fig. S3A). It is difficult to directly compare the potency of a small molecule and a biological agent in vivo. Nevertheless, this result directly demonstrated that the antitumor activity of TIC10 is superior to that of TRAIL when administered as single doses under these experimental conditions and

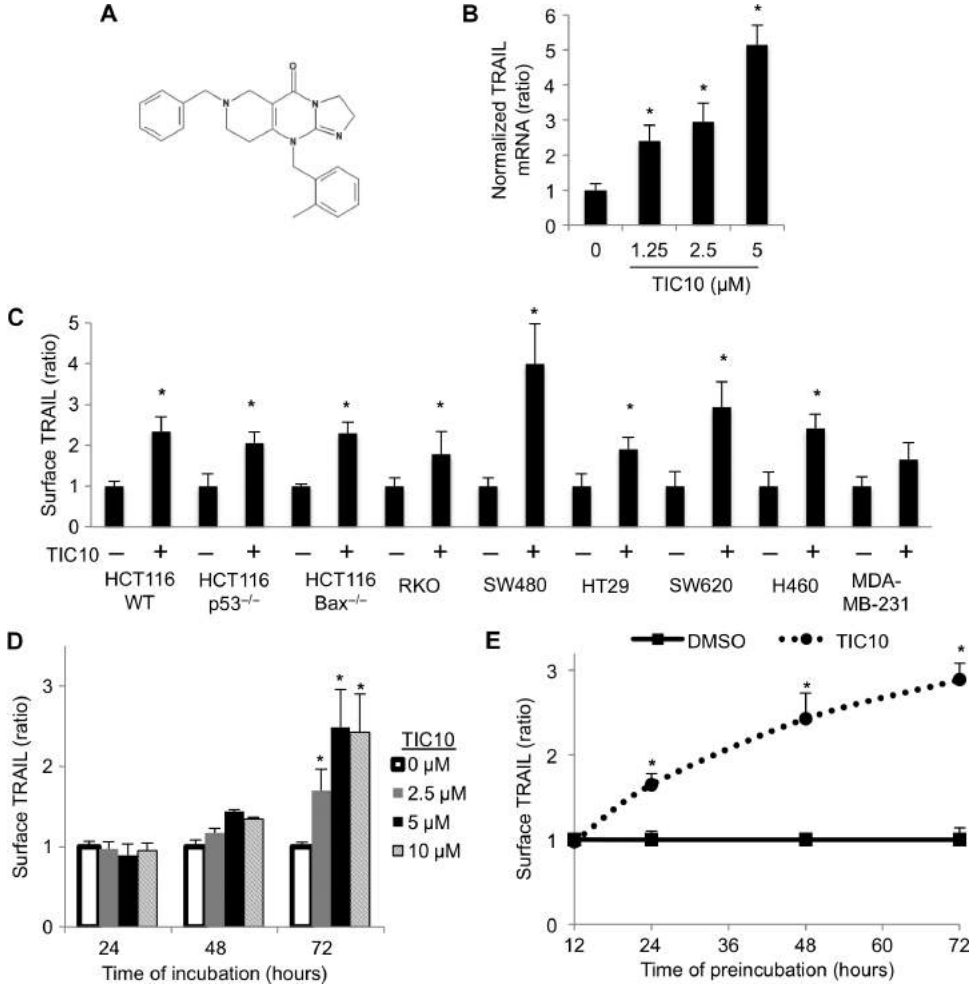

Fig. 1. TIC10 is a small molecule that induces TRAIL independent of p53. (**A**) Chemical structure of TIC10. (**B**) Quantitative reverse transcription polymerase chain reaction (qRT-PCR) analysis of TRAIL mRNA concentrations in HCT116 $p53^{-/-}$ cells (48 hours, $n = 4$). (**C**) Surface TRAIL induced by TIC10 in a panel of cancer cells (10 μM, 72 hours, $n = 3$). (**D**) Surface TRAIL in HCT116 $p53^{-/-}$ cells after TIC10 treatment at the indicated conditions and time points after treatment ($n = 3$). (**E**) HCT116 $p53^{-/-}$ TRAIL surface levels measured by flow cytometry at 72 hours after TIC10 treatment initiation (5 μM, $n = 3$). Cells were treated with TIC10 or dimethyl sulfoxide (DMSO) control for the indicated time of preincubation and then changed to a drug-free medium for the remaining period until analysis at 72 hours. Error bars indicate SD of replicates. *$P < 0.05$ between the indicated condition and controls.

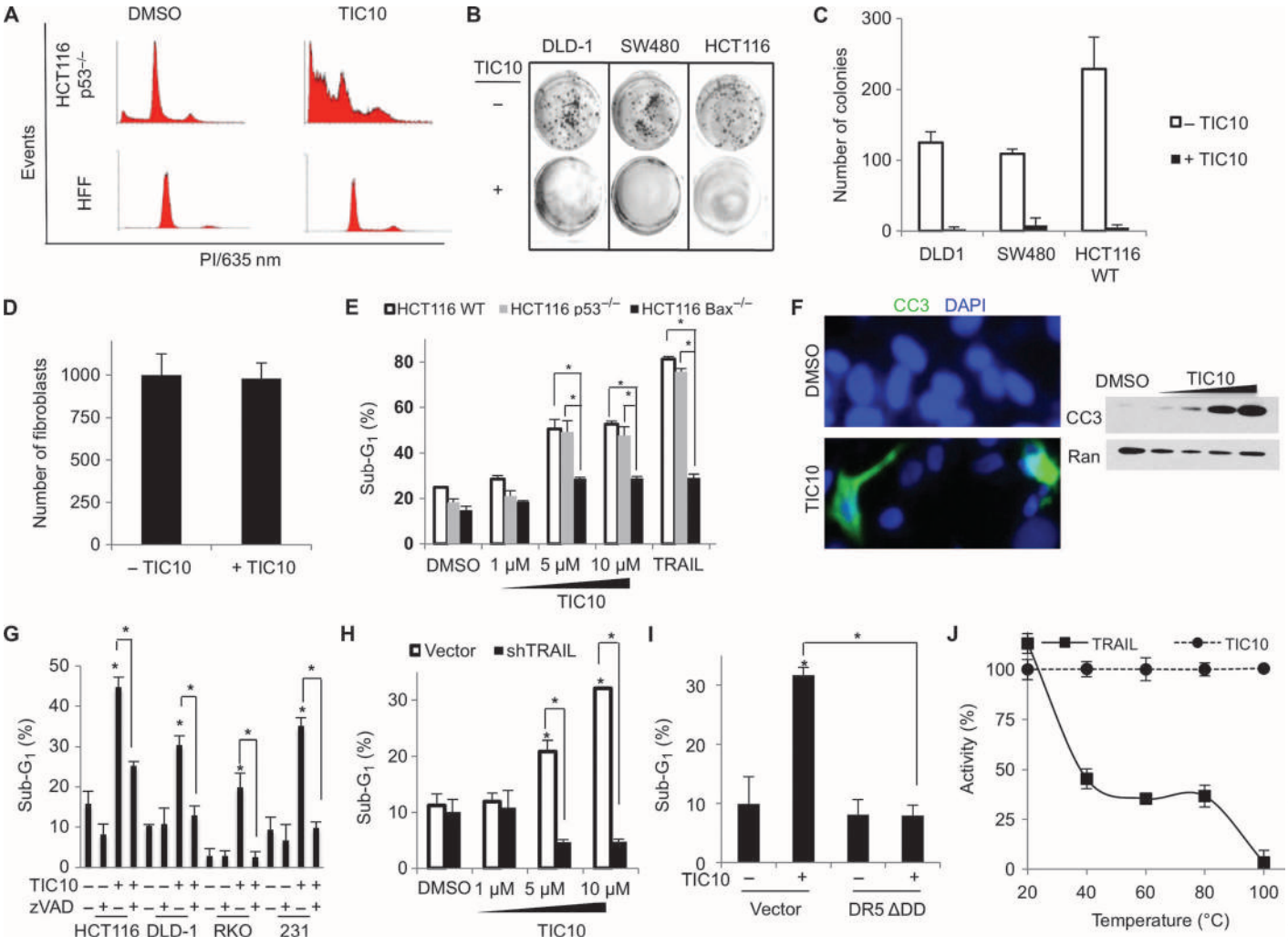

Fig. 2. TIC10 induces TRAIL-mediated apoptosis in vitro. (**A**) Cell cycle profiles of HCT116 p53$^{-/-}$and HFF cells treated with TIC10 (5 μM, 72 hours, $n = 3$). (**B** and **C**) Representative wells (B) and quantification of colony formation assays (C) of cancer cells per well with or without TIC10 (10 μM, 72 hours, $n = 3$). (**D**) Parallel experiments as in (C) but with HFF cells that were counted at the 72-hour endpoint ($n = 3$). (**E**) Percentage of sub-G_1 DNA (fragmented DNA indicative of cells undergoing apoptosis) in HCT116 wild-type (WT), p53$^{-/-}$, and Bax$^{-/-}$ cells after treatment with DMSO, TIC10 (1, 5, or 10 μM), or rhTRAIL (25 ng/ml) (72 hours, $n = 3$). (**F**) Cleaved caspase-3 (CC3) in HCT116 p53$^{-/-}$ cells assayed by immunofluorescence (left panel, 5 μM TIC10, caspase-3 shown in green) or Western blot analysis (right panel) treated with DMSO or TIC10 (1, 2.5, 5, and 10 μM) for 72 hours. (**G**) Percentage of sub-G_1 DNA in TIC10-treated cancer cells with or without preincubation with zVAD-fmk (10 μM, 72 hours, $n = 3$). (**H**) Percentage of sub-G_1 DNA in MDA-MB-231 cells with stable knockdown of TRAIL by shRNA treated with TIC10 (1, 5, and 10 μM) for 72 hours ($n = 3$). (**I**) Percentage of sub-G_1 DNA in H460 cells with endogenous DR5 or overexpressing a DR5 construct (DR5ΔDD) with its death domain replaced by enhanced green fluorescent protein (EGFP) (10 μM TIC10, 72 hours, $n = 3$). (**J**) Ability of TIC10 (5 μM) or TRAIL (25 ng/ml) to reduce cell viability in HCT116 cells after a 1-hour preincubation at the indicated temperatures (72 hours, $n = 3$). Error bars indicate SD of replicates. *$P < 0.05$ compared to control unless otherwise indicated.

acts, at least in part, through TRAIL produced by tumor cells. In DLD-1 colon cancer xenografts, TIC10 induced tumor stasis at 1 week after treatment, whereas TRAIL-treated tumors progressed after a single dose (fig. S3B). A single dose of TIC10 also induced a sustained regression of the SW480 xenograft and was equally effective when delivered by intraperitoneal or oral route, suggesting favorable oral bioavailability for TIC10 (fig. S3C). Titration of a single oral dose of TIC10 in the HCT116 xenograft model revealed sustained antitumor efficacy at 25 mg/kg (Fig. 3E). The lack of apparent toxicity at multiple doses delivered at fourfold above this therapeutic dose in previous xenografts, along with no adverse effects on body weight or liver histology (fig. S3, D to F), suggested that TIC10 has a wide therapeutic window. Exposure to oral TIC10 at 25 mg/kg weekly for 4 weeks in immunocompetent mice did not cause any changes in selected serum chemistry markers (table S1). We applied the same oral dosing schedule to Eμ-myc transgenic mice, which spontaneously develop metastatic lymphoma from weeks 9 to 12 of age, and found that TIC10 significantly ($P = 0.00789$) prolonged the survival of these mice by 4 weeks (Fig. 3F).

We then searched for cooperative combinations of TIC10 with approved chemotherapeutic agents. Among the tested chemotherapies, we observed potential in vitro synergy between TIC10 and the taxanes

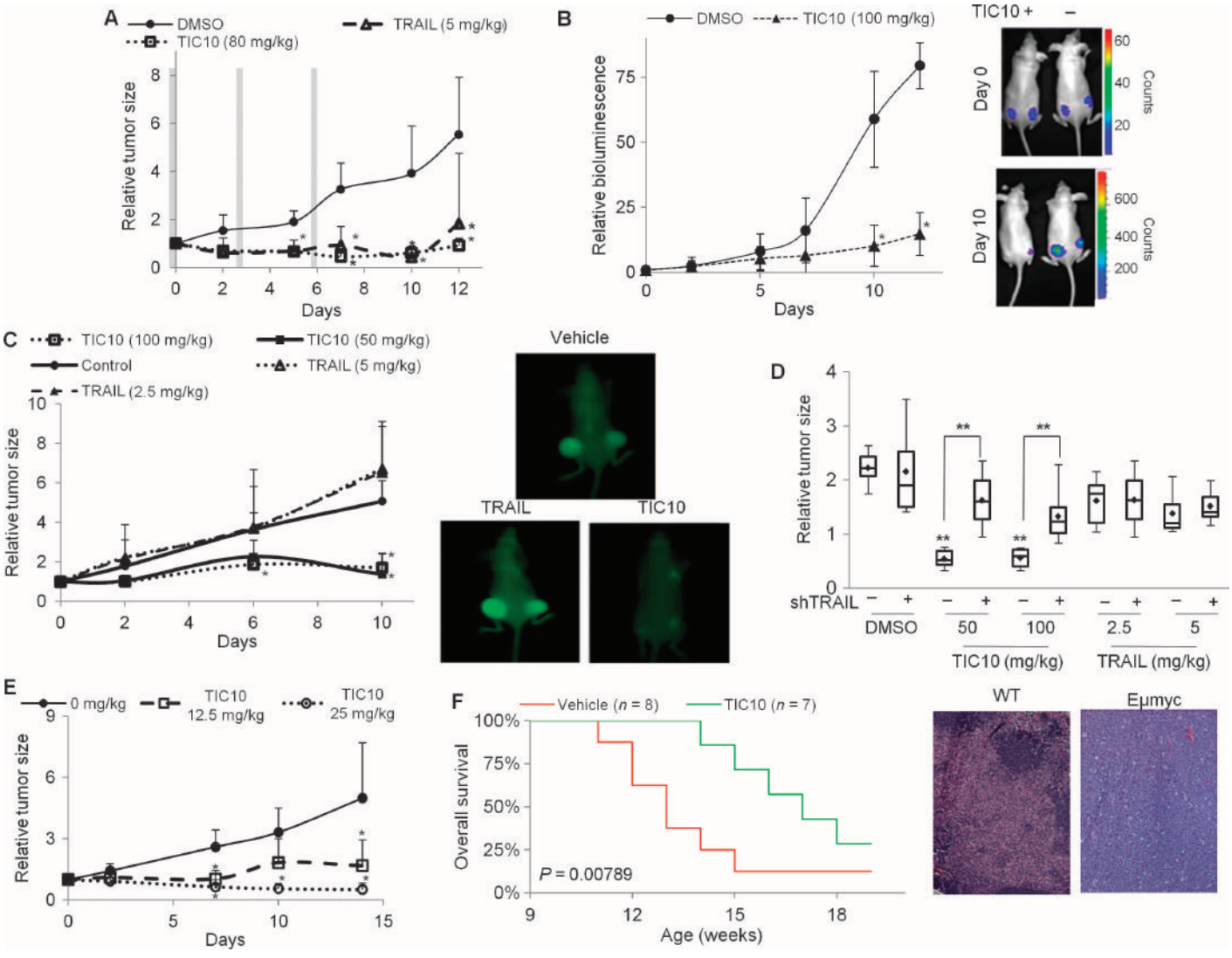

Fig. 3. TIC10 is a TRAIL-dependent antitumor agent in vivo. (**A**) Relative tumor size in mice bearing a HCT116 $p53^{-/-}$ xenograft and treated with three doses of TIC10 (intraperitoneal), TRAIL (intravenous), or vehicle (intraperitoneal) administered on days 0, 3, and 6 as indicated by gray vertical bars ($n = 10$). (**B**) Bioluminescence imaging of luciferase-expressing HCT116 $p53^{-/-}$ xenografts that received a single intraperitoneal injection of TIC10 or vehicle ($n = 6$). (**C**) Relative tumor size in RKO xenografts treated with a single dose of TIC10 (intraperitoneal), TRAIL (intravenous), or vehicle (intraperitoneal; $n = 10$). Right panel shows near-infrared images of sample mice from each cohort on day 13 after treatment and 3 days after injection with AngioSense 680. (**D**) Box and whisker plot of tumor volume on day 9 after treatment initiation in MDA-MB-231 xenografts expressing vector or shTRAIL and treated with single doses of TIC10 (intraperitoneal), TRAIL (intravenous), or vehicle (DMSO, intraperitoneal) ($n = 8$). (**E**) TIC10 or vehicle administered as a single oral dose in the HCT116 xenograft ($n = 6$). (**F**) Overall survival of Eμ-myc mice treated during weeks 9 to 12 with weekly single oral dose of TIC10 (25 mg/kg). Right panel shows hematoxylin and eosin (H&E) staining of axillary lymph nodes from Eμ-myc and WT C57/B6 mice at 14 weeks of age. *P* value was determined by log-rank test. For relative tumor volume plots, tumor size is expressed relative to the tumor size on day 0, which is defined as the day of treatment initiation. Error bars indicate SD of replicates. $^{*}P < 0.05$, $^{**}P < 0.005$, compared to control unless otherwise indicated.

paclitaxel and docetaxel (fig. S4, A to D). The combination of TIC10 and either of these taxanes cooperated to yield sustained cures for 10 days in the H460 non–small cell lung cancer xenograft (fig. S4, E to H). TIC10 also cooperated with bevacizumab when both were given once a week in a metastatic orthotopic mouse model of p53-deficient colorectal cancer. The combination reduced tumor burden at the primary cecal tumor and decreased spread to distal metastatic sites including the lung, liver, lymph nodes, and peritoneum (fig. S4, I and J). TIC10 alone and in combination with bevacizumab was well tolerated and caused no significant changes in body weight at the endpoint of this multidose regimen (fig. S4K).

TIC10 causes tumor-specific cell death by TRAIL-mediated direct and bystander effects

Immunohistochemical (IHC) analysis of TIC10-treated tumors revealed increased amounts of TRAIL and cleaved caspase-8, the initiator caspase involved in TRAIL-mediated apoptosis. Histological analysis and terminal deoxynucleotidyl transferase–mediated deoxyuridine

triphosphate nick end labeling (TUNEL) staining further confirmed that TIC10 induced apoptosis in the treated tumors (Fig. 4A). We also found that TIC10 induces TRAIL not only in the tumor but also in the stromal fibroblasts bordering the tumor (Fig. 4B). Quantification of TRAIL transcript revealed that TIC10 strongly increased TRAIL gene transcription in tumor xenografts at 48 to 108 hours after a single dose, which far exceeds the serum half-life of recombinant TRAIL (~30 min) (*22*) and matches the in vitro kinetics of TIC10 (Figs. 1D and 4C). Metabolic analysis of TIC10 in vitro indicated the presence of amine modifications that were not time-dependent (table S2). Metabolic analysis of serum TIC10 isolated from mice revealed a potential metabolite indicative of oxidation and glucuronide conjugation that was evident only at 8 hours after administration (table S3). Pharmacokinetic analysis revealed that TIC10 is quickly distributed and has a plasma half-life of ~6.5 hours (fig. S5 and table S4). Together, this suggests that TIC10 itself has a longer half-life than recombinant TRAIL and that the effects of TIC10 are temporally sustained for days in vivo and in vitro.

IHC analysis of normal tissues in TIC10-treated non–tumor-bearing mice revealed that TRAIL is up-regulated at the protein level in the brain, kidney, and spleen of mice without apparent toxicity as determined by histology (Fig. 4D). TRAIL up-regulation in response to TIC10 was not noted in other tissues including the liver at any time point (Fig. 4D).

We tested the effects of TIC10 on normal fibroblasts and found that TIC10 selectively induced apoptosis in p53-deficient tumor cells but not in normal fibroblasts in coculture experiments (Fig. 4E). TIC10 did induce a significant ($P < 0.05$) though modest amount of TRAIL on the surface of normal fibroblasts (Fig. 4F). Transplanting normal fibroblasts that were preincubated with TIC10 into a coculture with p53-deficient colon cancer cells resulted in a modest but significant ($P < 0.05$) increase in TRAIL-specific cell death of the cancer cell subpopulation (Fig. 4G). Together, these data indicate that TIC10 has a favorable therapeutic index and induces TRAIL in both tumor and normal cells, contributing to the antitumor efficacy of TIC10 through direct as well as bystander mechanisms.

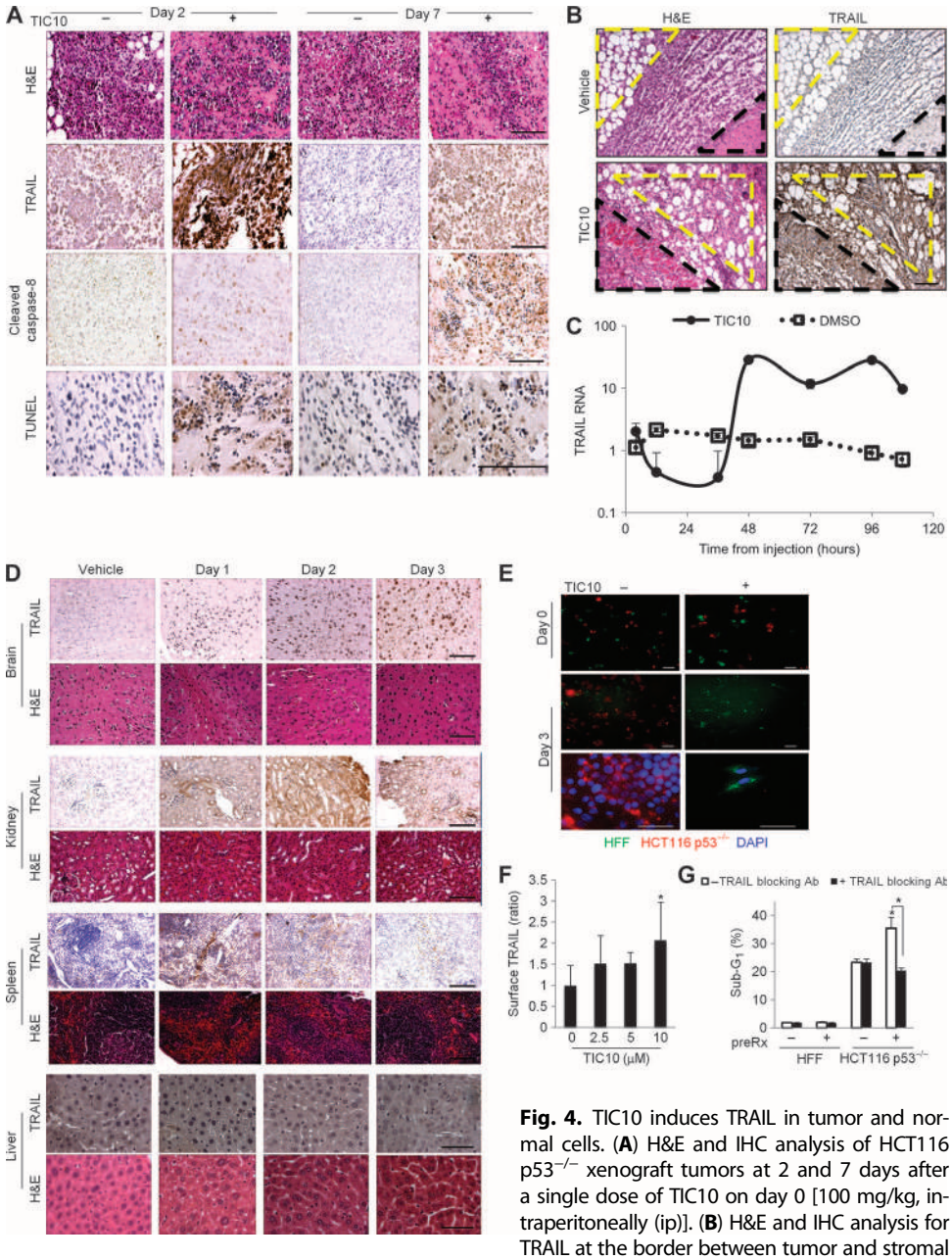

Fig. 4. TIC10 induces TRAIL in tumor and normal cells. (**A**) H&E and IHC analysis of HCT116 $p53^{-/-}$ xenograft tumors at 2 and 7 days after a single dose of TIC10 on day 0 [100 mg/kg, intraperitoneally (ip)]. (**B**) H&E and IHC analysis for TRAIL at the border between tumor and stromal fibroblasts from HCT116 $p53^{-/-}$ xenograft tumors after treatment with TIC10 (100 mg/kg, ip) or vehicle on day 2 after treatment. The yellow dashed lines indicate stromal fibroblasts, and the black dashed lines indicate the tumor. (**C**) qRT-PCR analysis of TRAIL transcript in HCT116 $p53^{-/-}$ xenograft tumors in athymic nude mice after a single dose of DMSO or TIC10 [25 mg/kg, intravenously (iv)] ($n = 4$). (**D**) Histological and TRAIL IHC analysis of normal tissue in athymic nude mice after TIC10 administration on day 0 (100 mg/kg, iv). (**E**) Coculture of HCT116 $p53^{-/-}$ and HFF cells labeled as red and green, respectively. TIC10 (10 μM)– or DMSO-treated wells are shown immediately before treatment or 3 days after treatment. The bottom two panels were taken at the 3-day endpoint after being counterstained with Hoechst. (**F**) Surface TRAIL analysis of HFF cells after TIC10 treatment (0, 2.5, 5, or 10 μM from left to right) (72 hours, $n = 3$). Surface TRAIL is shown relative to cells that were not treated with TIC10. (**G**) Percentage of sub-G_1 DNA in a coculture of HCT116 $p53^{-/-}$ cells and pretreated HFFs (24 hours, $n = 3$). HFF pretreatment consisted of a 72-hour incubation with TIC10 (10 μM) or DMSO. Coculture was in the presence or absence of the TRAIL-blocking antibody RIK-2. Scale bars, 100 μm. Error bars indicate SD of replicates. *$P < 0.05$, compared to control unless otherwise indicated.

TIC10 is an effective antitumor agent against orthotopic human glioblastoma multiforme tumors

The sustained induction of TRAIL in brain tissue suggested that the TIC10 small molecule can cross the intact blood-brain barrier, providing a clear advantage over a large protein such as TRAIL. We explored the possibility that TIC10 may serve as an antitumor agent against brain tumors. We first tested the activity of TIC10 in glioblastoma multiforme (GBM) cell lines and found that TIC10 induced TRAIL (Fig. 5A) and had a p53-independent GI_{50} (concentration that results in 50% growth inhibition) in the low micromolar range that is comparable with other cancer cell lines (Fig. 5B). We also found that TIC10 had substantial cytotoxic effects on freshly resected primary human GBM cells that are temozolomide-resistant and were previously irradiated. The tumor specimen was a grade IV glioblastoma with oligodendroglial component taken from a 38-year-old female patient who had undergone previous cytoreductive surgery and radiation (Fig. 5C). We tested TIC10 in preclinical models of GBM as a monoagent and in combination with bevacizumab on the basis of its favorable combination in the intracecal xenograft model (fig. S4, I to K). TIC10 exerted p53-independent cytotoxicity against a panel of GBM cell lines, including temozolomide-resistant GBM cell lines such as T98G, and induced a sustained regression of subcutaneous T98G xenografts to an extent similar to that of bevacizumab when given as a single oral dose (Fig. 5D). Furthermore, we found that a single dose of TIC10 doubled the overall survival of mice as a monoagent in an aggressive intracranial xenograft of human GBM with the SF767 cell

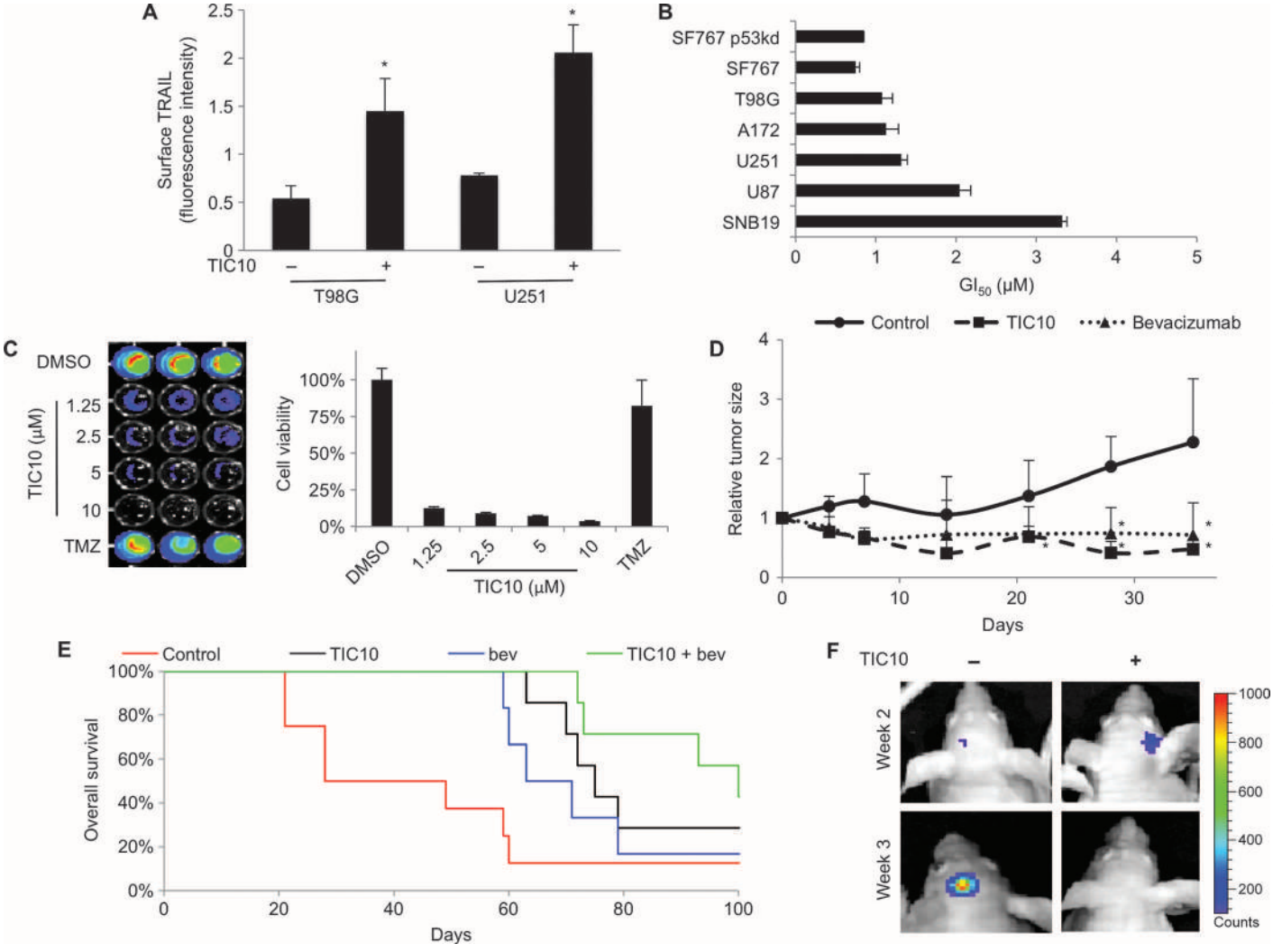

Fig. 5. TIC10 is effective as an antitumor agent in GBM. (**A**) Surface TRAIL in GBM cell lines after incubation with TIC10 (5 μM, 72 hours, $n = 3$). (**B**) GI_{50} values extrapolated from cell viability assays of the indicated GBM cell lines at 72 hours after treatment with TIC10 or DMSO ($n = 3$). (**C**) Cell viability assay of freshly resected glioblastoma tissue treated with DMSO, TIC10, or temozolomide (TMZ, 10 μM) (72 hours, $n = 3$). (**D**) Relative tumor size (compared to day 0) in a subcutaneous xenograft of T98G in mice treated with a single dose of vehicle, TIC10 (30 mg/kg, orally), or bevacizumab (10 mg/kg, iv) on day 0 ($n = 8$). (**E**) Overall survival of mice harboring SF767 intracranial tumors treated with a single oral dose of vehicle ($n = 8$), TIC10 (25 mg/kg, $n = 7$), bevacizumab (bev) (10 mg/kg, iv, $n = 6$), or TIC10 and bevacizumab ($n = 7$) at 2 weeks after implantation. (**F**) Bioluminescence imaging of a sample control mouse and a TIC10-treated mouse bearing an intracranial xenograft of SF767 glioblastoma. The bioluminescence scale bar on the right applies to all images in the panel. *$P < 0.05$ between the indicated condition and control.

line. It also cooperated with bevacizumab to triple the duration of survival of such brain tumor–bearing mice (Fig. 5, E and F, and table S5).

TIC10-induced TRAIL up-regulation is Foxo3a-dependent

We investigated gene expression profiles in TIC10-treated HCT116 $p53^{-/-}$ cells, revealing transcriptional changes in target genes of the FOXO family of transcription factors (Fig. 6A). This family includes Foxo3a, which has been previously shown to regulate the TRAIL gene promoter (*23*). We found that the FOXO target gene TRAIL receptor DR5 is up-regulated by TIC10 in tumors and several cancer cell lines and, to a much lesser extent, in normal cells (fig. S6, A to C). Regulation of FOXO family members is often achieved by changes in subcellular localization, such that transcriptional activity is correlated with nuclear localization. We found that among FOXO family members, Foxo3a (but not Foxo1a) undergoes a nuclear translocation in response to TIC10 (Fig. 6, B and C, and fig. S6, D and E). This is accompanied

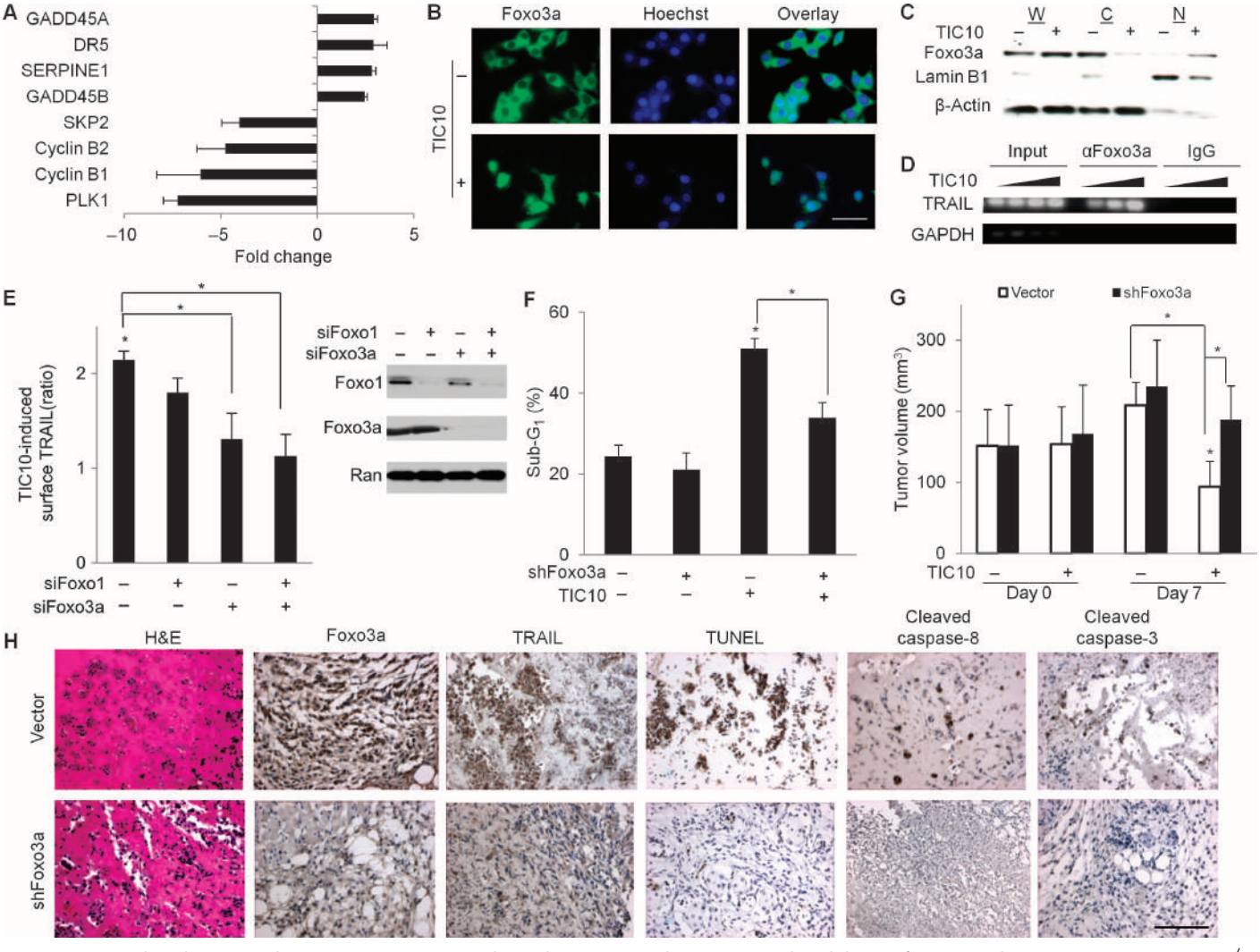

Fig. 6. TIC10-induced TRAIL and cytotoxicity are Foxo3a-dependent. (**A**) Transcriptional changes associated with FOXO signaling from gene expression profiling of HCT116 $p53^{-/-}$ cells at 48 hours after TIC10 treatment (10 μM) normalized to DMSO-treated cells (n = 3). $P < 0.05$ between DMSO and TIC10 treatment groups for all of these changes. (**B**) Immunofluorescence of Foxo3a in HCT116 cells with and without TIC10 treatment (48 hours, 10 μM). (**C**) Western blot analysis of whole-cell lysates (W) and cytoplasmic (C) and nuclear (N) extracts from HCT116 cells treated with DMSO or TIC10 (48 hours, 10 μM). β-Actin and lamin B1 are shown as cytoplasmic and nuclear loading controls, respectively. (**D**) ChIP assay for TIC10-induced translocation of Foxo3a to the TRAIL promoter at 48 hours after TIC10 treatment in HCT116 $p53^{-/-}$ cells (0, 2.5, 5, or 10 μM from left to right). (**E**) Flow cytometric analysis of cell surface TRAIL induced by TIC10 (10 μM) with or without transient knockdown of Foxo1 and/or Foxo3a in HCT116 $p53^{-/-}$ cells with siRNA (72 hours, n = 3). The cell surface TRAIL ratio refers to the amount of surface TRAIL in treated cells relative to that in cells that were not treated with TIC10. Confirmation of knockdown is shown by Western blot analysis (right). (**F**) Percentage of sub-G_1 DNA in HCT116 cells with or without stable knockdown of Foxo3a and with or without TIC10 treatment (10 μM, 72 hours, n = 3). (**G**) Tumor volume of HCT116 xenograft with or without stable knockdown of Foxo3a by shRNA after a single oral dose of vehicle or TIC10 (25 mg/kg) on day 0 (n = 10). (**H**) IHC analysis and TUNEL staining of HCT116 tumors with or without stable knockdown of Foxo3a 3 days after a single dose of TIC10 (25 mg/kg, orally). Scale bars, 100 μm. Error bars indicate SD of replicates. *$P < 0.05$, compared to control unless otherwise indicated.

by a dose-dependent increase in the amount of Foxo3a localized to the TRAIL promoter as shown by a chromatin immunoprecipitation (ChIP) assay (Fig. 6D). Transient knockdown of Foxo3a and Foxo1 revealed that Foxo3a specifically mediates TIC10-induced TRAIL up-regulation (Fig. 6E). Stable knockdown of Foxo3a significantly inhibited TIC10-induced up-regulation of TRAIL production and subsequent tumor cell death (Fig. 6F and fig. S6F). Furthermore, overexpression of a plasmid encoding for a mutant Foxo3a lacking its DNA binding domain blunted the transcriptional induction of TRAIL in response to TIC10 (fig. S6G). Stable knockdown of Foxo3a in tumor cells also significantly ($P < 0.05$) inhibited the antitumor activity of TIC10 and TIC10-induced hallmarks of TRAIL-mediated apoptosis in tumors in vivo (Fig. 6, G and H).

Dual inactivation of Akt and ERK by TIC10 cooperatively induces TRAIL

We explored TIC10-induced changes in previously described regulators of Foxo3a, such as IKK (*24*, *25*), Akt (*26*), and ERK (*20*, *27*) (Fig. 7A). We found that both pAkt and pERK are down-regulated by TIC10 treatment in a dose-dependent manner. This decrease in pAkt and pERK is accompanied by dephosphorylation of the sites they phosphorylate on Foxo3a. TIC10 also caused a down-regulation of the total expression of ERK (fig. S7A). We found that ERK mRNA was unaffected, whereas the protein stability of ERK decreased in response to TIC10 (fig. S7, B and C). The inhibition of Akt and ERK activity is indirect, as confirmed by in vitro kinase activity assays (fig. S7D). We found that Akt myristoylation can counteract the cytotoxic response to TIC10, including TRAIL up-regulation and the nuclear translation of Foxo3a, and that overactivating Akt can suppress even basal expression of TRAIL (fig. S7, E to G). A time-course analysis revealed that TIC10-induced inactivation of Akt and ERK occurs after 48 hours, in concert with the kinetics of dephosphorylation of Foxo3a and TRAIL up-regulation (Fig. 7B and fig. S7H). These effects were also observed in TIC10-treated xenograft tumors in vivo (Fig. 7C) and in several human cancer cell lines of different tumor types with diverse genetic alterations (Fig. 7D).

We hypothesized that dual inhibition of the phosphoinositide 3-kinase/Akt and the mitogen-activated protein kinase (MAPK) pathways will cooperatively lead to the nuclear translocation of Foxo3a and ensuing TRAIL up-regulation. We found that A6730 and U0126 monoethanolate, which are inhibitors of Akt1/2 (*28*) and MEK (mitogen-activated or extracellular signal–regulated protein kinase kinase) (*29*), respectively, cooperatively induce Foxo3a-dependent TRAIL up-regulation and lead to TRAIL-mediated cell death (Fig. 7E and fig. S7, I and K). These observations were corroborated by small interfering RNA (siRNA) experiments, revealing that ERK and Akt can be inhibited to cooperatively up-regulate TRAIL gene expression (Fig. 7, F and G, and fig. S7L).

We next examined the effects of TIC10 on the MAPK signaling pathway. TIC10 does not affect the phosphorylation or expression of epidermal growth factor receptor (EGFR), B-Raf, or C-Raf (Fig. 7, H and I, and fig. S8, A to D). However, the phosphorylation of MEK and ERK is abolished in response to TIC10 even when the drug is washed out, unlike the EGFR inhibitor gefitinib. The dephosphorylation of MEK and ERK in response to TIC10 was not affected by treatment with okadaic acid, which inhibits phosphatases (fig. S8E). These findings suggest that TIC10 indirectly inhibits the MAPK signaling pathway at the level of MEK and its downstream targets. Together, these data indicate that TIC10 causes a dual inactivation of Akt and ERK, which leads to the translocation of their mutual substrate Foxo3a into the nucleus, where it transcriptionally induces the TRAIL gene to activate cell death and antitumor effects in vivo (Fig. 8).

DISCUSSION

Our findings demonstrate that TIC10 is a safe and orally active antitumor agent that has potent cancer-specific cytotoxicity through sustained stimulation of the endogenous TRAIL tumor suppressor by normal and tumor tissues, including the brain. TIC10 induces TRAIL in a Foxo3a-dependent manner, which also up-regulates TRAIL death receptor DR5 among other targets, potentially allowing for sensitization of some TRAIL-resistant tumor cells. Our observations demonstrate that pharmacological activation of Foxo3a is a powerful antitumor strategy that requires TRAIL as a proapoptotic effector target gene, and that Foxo3a activation through dual inhibition of Akt and ERK is achievable by the single small-molecule TIC10. The induction of TRAIL caused by TIC10 is sustained in both tumor and host cells, and in vitro evidence suggests that these normal host cells contribute to TIC10-induced cancer cell death through a bystander effect.

TIC10 has broad-spectrum activity that we demonstrated in primary patient samples and cell lines resistant to conventional therapies. This bodes well for the clinical utility of TIC10, as its activity does not rely exclusively on molecules that are commonly altered in cancer, such as EGFR, Her2, KRAS, p53, or PTEN. This is in agreement with a previous study describing the utility of Foxo3a activation as an anticancer mechanism that targets cancer cells that are resistant to therapies inhibiting upstream regulators of MAPK signaling (*30*). The elucidation of the mechanism of TIC10 yields important information for the clinical translation of this molecule, as it allows for the identification of resistance mechanisms such as overactivated Akt, which we demonstrate directly. Additionally, it suggests that pERK, pAkt, Foxo3a localization and phosphorylation, as well as cell surface and serum TRAIL can be tracked to monitor the effectiveness of TIC10 in clinical trials.

The use of small molecules to induce an endogenous gene in lieu of administering a recombinant protein is a promising therapeutic approach. Our study demonstrates that limitations of a therapeutic recombinant protein such as TRAIL, including biodistribution and pharmacokinetic properties, can be effectively overcome through the use of a small molecule. Furthermore, a secreted protein such as TRAIL may be a particularly well-suited target for such a strategy because normal cells at sites outside the tumor can produce soluble or cell-bound TRAIL protein that may contribute to the therapeutic response via a bystander mechanism. TRAIL-mediated bystander effects with normal cells have previously been reported in response to radiation and may represent a promising therapeutic opportunity to augment efficacy (*31*). This strategy has the potential to produce large quantities of antitumor proteins as the trillions of cells in the human body universally harbor the potential to produce endogenous proteins in a temporally sustained fashion.

The bystander protein production strategy must be used carefully because normal cells must maintain their normal function and the target protein must be nontoxic to the normal cells, as is the case for TRAIL (*32*). Additionally, the pleiotropic effects of the small molecule must also be considered because they have the potential to cause toxicity or increase efficacy through cooperative mechanisms, such as

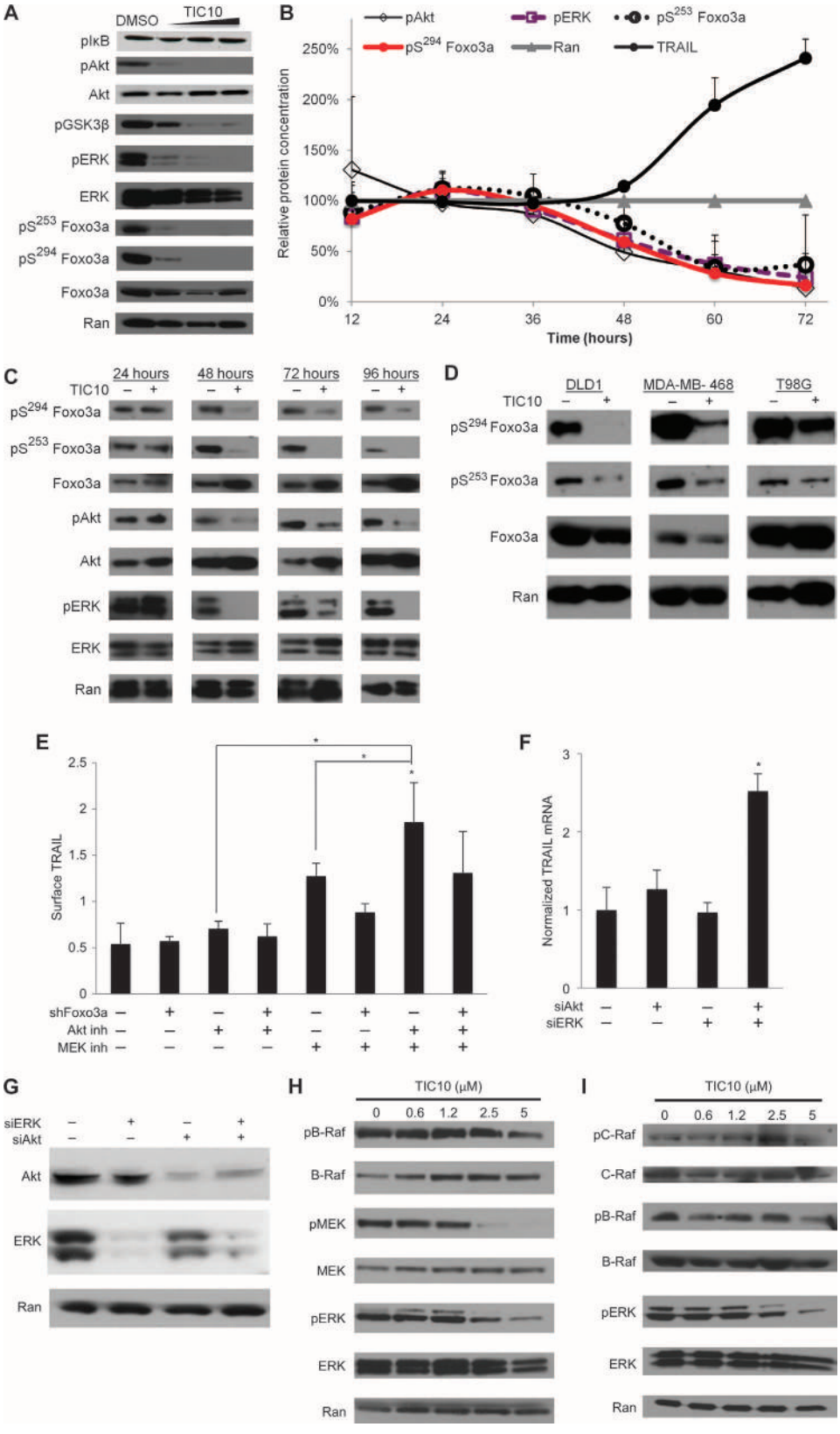

Fig. 7. TIC10 inactivates Akt and ERK to induce TRAIL through Foxo3a. (**A**) Western blot analysis of HCT116 p53$^{-/-}$ cells treated with TIC10 (2.5, 5, and 10 μM) for 72 hours. (**B**) Time course of TIC10-induced effects determined by densitometry of Western blot analysis of HCT116 p53$^{-/-}$ cells treated with TIC10 (5 μM) or DMSO (n = 3). Data are expressed relative to the control sample for each time point and normalized to Ran as a loading control. TRAIL was quantified by flow cytometry as a parallel experiment (n = 3). (**C**) Western blot analysis of HCT116 p53$^{-/-}$ xenograft tumors in athymic nude mice after a single dose of DMSO or TIC10 (25 mg/kg, iv) (**D**) Western blot analysis of TIC10-induced effects on Foxo3a in DLD-1 human colon cancer, MDA-MB-468 human breast cancer, and T98G human GBM cell lines (10 μM, 72 hours). (**E**) Flow cytometric analysis of TRAIL in HCT116 p53$^{-/-}$ cells after incubation with 10 μM A6730 (Akt inhibitor), U0126 monoethanolate (MEK inhibitor), or both (48 hours), with or without stable knockdown of Foxo3a (n = 3). (**F**) qRT-PCR analysis of TRAIL mRNA at 48 hours after transient knockdown of Akt and/or ERK in HCT116 p53$^{-/-}$ cells (n = 3). For siERK and siAkt combination, $P < 0.05$ compared to all other conditions. (**G**) Confirmation of Akt and ERK knockdown by Western blot analysis. (**H**) Western blot analysis of B-Raf/MEK/ERK signaling in HCT116 cells treated with TIC10 at the indicated concentrations (48 hours). (**I**) Western blot analysis of Raf expression and phosphorylation in HCT116 cells treated with TIC10 at the indicated concentrations (48 hours). Error bars indicate SD of replicates. *$P < 0.05$, compared to control unless otherwise indicated.

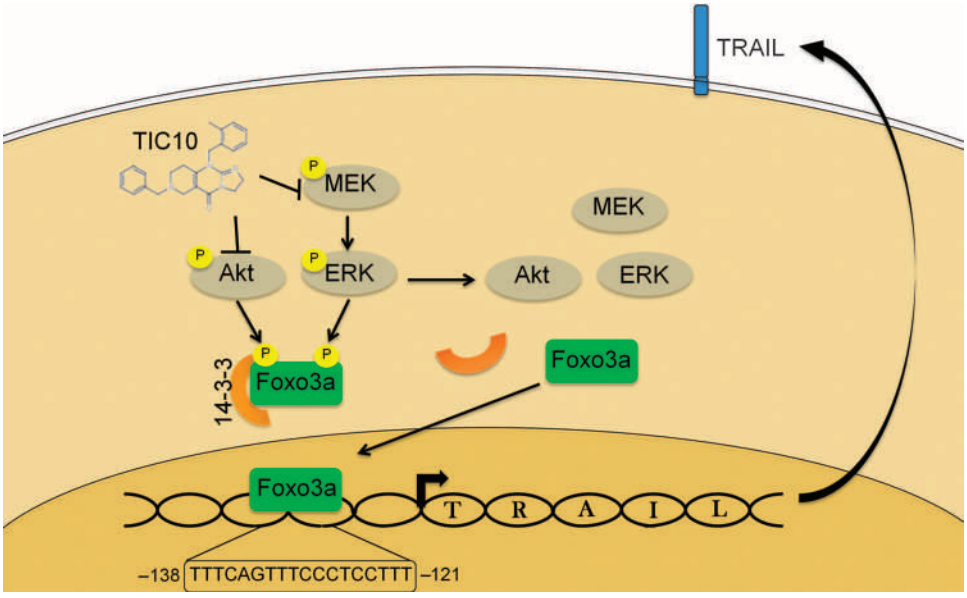

Fig. 8. TIC10 up-regulates TRAIL through inhibition of Akt and MEK/ERK and activation of Foxo3a. TIC10 causes inactivation of the prosurvival kinases MEK, ERK, and Akt. ERK and Akt normally phosphorylate Foxo3a at S^{253} and S^{294}, respectively. These phosphorylation events create docking sites for 14-3-3 proteins that bind Foxo3a and sequester it in the cytoplasm, thereby inhibiting its activity as a transcription factor. Through its actions on Akt and ERK, TIC10 inhibits Foxo3a phosphorylation, which allows Foxo3a to translocate to the nucleus and bind to the TRAIL promoter that harbors a FOXO binding site. This binding stimulates TRAIL gene transcription and translation, increasing the amount of TRAIL on the cell surface.

the concomitant DR5 up-regulation observed in tumor cells in response to TIC10.

One limitation of this study is that although we demonstrate that TIC10 requires TRAIL for its apoptotic activity, other targets of Akt, MEK, and ERK may contribute to its substantial antitumor activity. Previous reports have described several FOXO-induced changes in genes that mediate TRAIL sensitivity, including DR5 up-regulation as well as down-regulation of FLIP (*33*, *34*), although we did not observe the latter in our gene expression profiling of changes in response to TIC10. Thus, the increased spectrum of activity and antitumor effects gained with TIC10 relative to TRAIL treatment cannot be exclusively ascribed to the induction of only the TRAIL gene by TIC10. More studies will be needed to further elucidate the mechanism of action of TIC10, including its direct binding target. Medicinal chemistry with TIC10 may be explored to clarify structure-activity relationships and to identify a more potent compound that maintains the wide therapeutic window of TIC10. Another limitation of this study is that while the safety of TIC10 was evaluated in vitro and in vivo, the identification of adverse events and a complete safety study in nonrodent species will need to be executed before clinical testing. Finally, the efficacy comparisons between TRAIL and TIC10 in this study are confounded by difficulties associated with comparing the potency of biological agents and small molecules. Whereas the preclinical activity of TIC10 is promising and outperforms TRAIL in some preclinical studies, controlled comparisons of clinical activity are needed to truly assess the superiority of the compound.

Small molecules have targeted other members of the FOXO family, for example, to induce the nuclear translocation of Foxo1 (*35*). The identification of Foxo3a as the transcription factor and TRAIL as the apoptotic effector for TIC10-induced therapeutic effects has implications that extend beyond the small molecule itself. Our observations strongly argue that TRAIL plays an essential role in the apoptotic response induced by Foxo3a, which is a promising drug target and accessible cellular mechanism for inducing the TRAIL gene. The conservation of the Foxo3a-dependent mechanism of TIC10 in the presence of diverse upstream oncogenic alterations holds promising therapeutic potential. The Akt- and ERK-dependent mechanism of TIC10 is in full agreement with a recent report supporting that the dual inactivation of Akt and MAPK signaling pathways in mutant KRAS cancer cells is a potent and cooperative strategy (*36*). Our observations suggest that the Foxo3a/TRAIL axis may play a critical role in apoptosis associated with dual inhibition of Akt and ERK, and that the combination of approved antitumor agents targeting indirectly these two pathways should be explored in an effort to gain Foxo3a/TRAIL-dependent activity. Our findings also highlight TRAIL as an important target of Foxo3a and are in congruence with a recent report arguing that Foxo3a-dependent TRAIL is responsible for HIV-induced apoptosis of memory B cells (*37*). The observation that Foxo3a rather than Foxo1, which has been previously targeted by small molecules (*35*), specifically regulates the TIC10-induced response lends credence to the notion that different members of the FOXO family of transcription factors play distinct roles.

The induction of TRAIL by histone deacetylase inhibitors such as vorinostat has been reported (*38*). In addition, there are several other TRAIL-based therapies that are being investigated, such as the TRAIL receptor agonist antibodies lexatumumab and mapatumumab, proteins engineered to mimic the proapoptotic effects of TRAIL on the death receptors (*13*), and adenovirus-delivered TRAIL (*39*). We posit that the mechanism of TIC10, its spectrum of activity, and drug properties make TIC10 a promising alternative with some advantages. The requirement of TRAIL for activity, bystander effects, bioavailability, biodistribution, stability, and concomitant up-regulation of DR5 by TIC10 cumulatively position TIC10 as an attractive therapeutic approach aimed at using the apoptotic potential of TRAIL with demonstrable advantages over currently available TRAIL pathway–based therapies.

TIC10 is an anticancer therapy that provides an excellent opportunity for modulation of host antitumor responses and the pharmacokinetic properties of an endogenous antitumor protein. Moreover, the pharmacological induction of TRAIL in the brain demonstrates a therapeutic approach in brain malignancies otherwise refractory to current therapies and an alternative solution for the general limitations of exogenous protein delivery. TIC10 offers an effective cancer therapeutic strategy that uses both normal and tumor cells to endogenously produce an antitumor agent via conserved signaling. The modulation

of pharmacokinetic properties of endogenous TRAIL as a tumor-suppressive agent by a small molecule such as TIC10 suggests that exploration of pharmacological induction/pharmacokinetic tuning of other endogenous antitumor proteins is feasible and warranted. The molecular mechanism of TIC10 also suggests that the antitumor effects of Foxo3a and the TRAIL receptor pathway can be harnessed through the dual inhibition of Akt and ERK, which should be explored with targeted agents in clinical development.

MATERIALS AND METHODS

Reagents and cell-based assays

All cell lines were obtained from the American Type Culture Collection, except for the HCT116 $Bax^{-/-}$ and HCT116 $p53^{-/-}$ cells (gifts from B. Vogelstein, Johns Hopkins University) and GBM cell lines (provided by A. Mintz, Wake Forest University). Lentiviral infection was performed with MDA-MB-231 cells and TRAIL shRNA or vector and HCT116 with Foxo3a shRNA or vector purchased from Sigma-Aldrich. H460 DR5ΔDD-EGFP cells were constructed with complementary DNA coding for a DR5 fragment without a death domain by inserting amino acids 1 to 298 of the human DR5 gene into the pEGFP-N1 vector to express a DR5(1–298) fusion protein. The fusion construct was transfected into H460 cells with Lipofectamine 2000 (Invitrogen) and selected with G418. Positive clones were verified by fluorescence microscopy and Western blot analysis. TIC10 (NSC350625) was obtained from the NCI Developmental Therapeutic Program. A6730 and U0126 monoethanolate were obtained from Sigma. Purified, recombinant TRAIL was produced as previously described (*40*). The RIK-2 antibody (Santa Cruz Biotechnology) was used at 1 μg/ml and zVAD-fmk (Promega) was used at 20 μM.

Flow cytometry and cell death assays

Floating and adherent cells were analyzed on a Coulter-Beckman Elite Epics cytometer. For surface TRAIL experiments, adherent cells were harvested by brief trypsinization, fixed in 4% paraformaldehyde in phosphate-buffered saline (PBS) for 20 min, incubated with an anti-TRAIL antibody (Abcam, ab2435) at 1:250 overnight, washed and incubated with anti-rabbit Alexa Fluor 488 (Invitrogen) for 30 min, and analyzed. Cells were gated on forward and side scatter to eliminate debris and dead cells from the analysis. Surface TRAIL data are expressed as median fluorescence intensity relative to that of control samples unless indicated otherwise. Surface DR5 was analyzed similarly with an antibody from Imgenex. For sub-G_1 content and cell cycle profile analysis, all cells were pelleted and ethanol-fixed, followed by staining with propidium iodide (Sigma) in the presence of RNase. Cell viability assays were carried out in 96-well black-walled clear-bottom plates with CellTiter-Glo (Promega) according to the manufacturer's protocols.

Colony formation assays

The indicated cell lines were plated at 500 cells per well and allowed to adhere, and then treated the next day in fresh complete medium. At 3 days after treatment, the medium was replaced with drug-free medium and cells were propagated for 10 days, with fresh medium given once every 3 days. At the end of the 10-day period, cells were washed in PBS, fixed with methanol, stained with Coomassie blue, rinsed, and dried for quantification.

Western blot analysis

Western blot analysis was conducted as previously described (*41*) with NuPAGE 4 to 12% bis-tris gel and visualized with SuperSignal West Femto (Thermo Scientific) and x-ray film. Densitometry was performed with NIH ImageJ. Nuclear and cytoplasmic extracts were prepared with a cytoplasmic lysis buffer (10 mM Hepes, 10 mM KCl, 2 mM $MgCl_2$, 1 mM dithiothreitol) followed by a nuclear lysis buffer (20 mM Hepes, 420 mM NaCl, 1.5 mM $MgCl_2$, 250 μM EDTA, 25% glycerol). For all lysis buffers, fresh protease inhibitor (Roche) and 1 mM sodium orthovanadate were added immediately before use.

Primary specimens

All primary patient specimens were obtained in accordance with the Institutional Review Board at Penn State Hershey Medical Center under approved protocols. Samples were received immediately after resection, manually digested in complete Dulbecco's modified Eagle's medium (DMEM), filtered with a 100-μm nylon mesh, and plated at 2×10^5 cells/ml in complete DMEM for the described experiments.

In vivo studies

All animal experiments were conducted in accordance with the Institutional Animal Care and Use Committee at the Pennsylvania State University College of Medicine. For subcutaneous xenografts, 4- to 6-week-old female athymic nu/nu mice (Charles River Laboratories) were inoculated with 1×10^6 cells (2.5×10^6 for T98G) of the indicated cell lines in each rear flank as a 200-μl suspension of 1:1 Matrigel (BD)/PBS. All subcutaneous tumors were allowed to establish for 1 to 4 weeks after injection until reaching a volume of ~125 mm^3 before treatment initiation. Other experimental details are outlined in Supplementary Materials.

ChIP assays

ChIP assays were carried out as previously described for the TRAIL promoter (*38*) with a ChIP-grade antibody for Foxo3a (Abcam) or an equivalent concentration of rabbit immunoglobulin G (SouthernBiotech) as a nonspecific control.

Statistical analyses

For pairwise comparisons, we analyzed the data using Student's two-tailed *t* test in Excel (Microsoft). Log-rank statistical analysis was performed with a Web-based script that interfaces with the statistical package R (http://bioinf.wehi.edu.au/software/russell/logrank/).

SUPPLEMENTARY MATERIALS

www.sciencetranslationalmedicine.org/cgi/content/full/5/171/171ra17/DC1

Materials and Methods

Fig. S1. TIC10 structure was confirmed by mass spectrometry.

Fig. S2. TIC10 exhibits broad-spectrum and TRAIL-specific activity in vitro.

Fig. S3. TIC10 induces TRAIL-mediated apoptosis and is nontoxic in vivo.

Fig. S4. TIC10 cooperates with taxanes and bevacizumab.

Fig. S5. The pharmacokinetics of TIC10 were analyzed in tumor-free mice.

Fig. S6. TIC10 up-regulates DR5 and induces Foxo3a activity by stimulating nuclear translocation.

Fig. S7. Akt and ERK are indirectly inhibited by TIC10 and affect TIC10-induced TRAIL signaling and cell death.

Fig. S8. TIC10 indirectly inhibits the MAPK pathway downstream of EGFR.

Table S1. The serum chemistry of C57/B6 mice treated with TIC10 (25 mg/kg) weekly for 4 weeks was unchanged compared to vehicle-treated mice ($n = 3$).

Table S2. TIC10 metabolites in vitro varied over time.

Table S3. Plasma metabolites from mice treated with TIC10 were analyzed by mass spectrometry.

Table S4. The pharmacokinetics of TIC10 were analyzed in the plasma of C57/B6 mice.
Table S5. Overall survival of mice with SF767 intracranial tumors improved with TIC10 and bevacizumab treatment.

REFERENCES AND NOTES

1. G. Pan, K. O'Rourke, A. M. Chinnaiyan, R. Gentz, R. Ebner, J. Ni, V. M. Dixit, The receptor for the cytotoxic ligand TRAIL. *Science* **276**, 111–113 (1997).
2. G. Pan, J. Ni, Y. F. Wei, G. Yu, R. Gentz, V. M. Dixit, An antagonist decoy receptor and a death domain-containing receptor for TRAIL. *Science* **277**, 815–818 (1997).
3. G. S. Wu, T. F. Burns, E. R. McDonald III, W. Jiang, R. Meng, I. D. Krantz, G. Kao, D. D. Gan, J. Y. Zhou, R. Muschel, S. R. Hamilton, N. B. Spinner, S. Markowitz, G. Wu, W. S. El-Deiry, *KILLER/DR5* is a DNA damage-inducible p53-regulated death receptor gene. *Nat. Genet.* **17**, 141–143 (1997).
4. A. Ashkenazi, Targeting death and decoy receptors of the tumour-necrosis factor superfamily. *Nat. Rev. Cancer* **2**, 420–430 (2002).
5. F. A. Greco, P. Bonomi, J. Crawford, K. Kelly, Y. Oh, W. Halpern, L. Lo, G. Gallant, J. Klein, Phase 2 study of mapatumumab, a fully human agonistic monoclonal antibody which targets and activates the TRAIL receptor-1, in patients with advanced non-small cell lung cancer. *Lung Cancer* **61**, 82–90 (2008).
6. D. R. Camidge, R. S. Herbst, M. S. Gordon, S. G. Eckhardt, R. Kurzrock, B. Durbin, J. Ing, T. M. Tohnya, J. Sager, A. Ashkenazi, G. Bray, D. Mendelson, A phase I safety and pharmacokinetic study of the death receptor 5 agonistic antibody PRO95780 in patients with advanced malignancies. *Clin. Cancer Res.* **16**, 1256–1263 (2010).
7. T. Trarbach, M. Moehler, V. Heinemann, C. H. Köhne, M. Przyborek, C. Schulz, V. Sneller, G. Gallant, S. Kanzler, Phase II trial of mapatumumab, a fully human agonistic monoclonal antibody that targets and activates the tumour necrosis factor apoptosis-inducing ligand receptor-1 (TRAIL-R1), in patients with refractory colorectal cancer. *Br. J. Cancer* **102**, 506–512 (2010).
8. C. H. Mom, J. Verweij, C. N. Oldenhuis, J. A. Gietema, N. L. Fox, R. Miceli, F. A. Eskens, W. J. Loos, E. G. de Vries, S. Sleijfer, Mapatumumab, a fully human agonistic monoclonal antibody that targets TRAIL-R1, in combination with gemcitabine and cisplatin: A phase I study. *Clin. Cancer Res.* **15**, 5584–5590 (2009).
9. S. Leong, R. B. Cohen, D. L. Gustafson, C. J. Langer, D. R. Camidge, K. Padavic, L. Gore, M. Smith, L. Q. Chow, M. von Mehren, C. O'Bryant, S. Hariharan, S. Diab, N. L. Fox, R. Miceli, S. G. Eckhardt, Mapatumumab, an antibody targeting TRAIL-R1, in combination with paclitaxel and carboplatin in patients with advanced solid malignancies: Results of a phase I and pharmacokinetic study. *J. Clin. Oncol.* **27**, 4413–4421 (2009).
10. R. Plummer, G. Attard, S. Pacey, L. Li, A. Razak, R. Perrett, M. Barrett, I. Judson, S. Kaye, N. L. Fox, W. Halpern, A. Corey, H. Calvert, J. de Bono, Phase 1 and pharmacokinetic study of lexatumumab in patients with advanced cancers. *Clin. Cancer Res.* **13**, 6187–6194 (2007).
11. A. W. Tolcher, M. Mita, N. J. Meropol, M. von Mehren, A. Patnaik, K. Padavic, M. Hill, T. Mays, T. McCoy, N. L. Fox, W. Halpern, A. Corey, R. B. Cohen, Phase I pharmacokinetic and biologic correlative study of mapatumumab, a fully human monoclonal antibody with agonist activity to tumor necrosis factor–related apoptosis-inducing ligand receptor-1. *J. Clin. Oncol.* **25**, 1390–1395 (2007).
12. E. Bremer, W. Helfrich, A better TRAIL variant for tumor cell-specific targeting?—Letter. *Mol. Cancer Ther.* **9**, 2853 (2010).
13. J. E. Allen, R. Ferrini, D. T. Dicker, G. Batzer, E. Chen, D. I. Oltean, B. Lin, M. W. Renshaw, A. Kretz-Rommel, W. S. El-Deiry, Targeting TRAIL death receptor 4 with trivalent DR4 Atrimer complexes. *Mol. Cancer Ther.* **11**, 2087–2095 (2012).
14. L. G. Menon, K. Kelly, H. W. Yang, S. K. Kim, P. M. Black, R. S. Carroll, Human bone marrow-derived mesenchymal stromal cells expressing S-TRAIL as a cellular delivery vehicle for human glioma therapy. *Stem Cells* **27**, 2320–2330 (2009).
15. K. Kuribayashi, G. Krigsfeld, W. Wang, J. Xu, P. A. Mayes, D. T. Dicker, G. S. Wu, W. S. El-Deiry, TNFSF10 (TRAIL), a p53 target gene that mediates p53-dependent cell death. *Cancer Biol. Ther.* **7**, 2034–2038 (2008).
16. S. Ghaffari, Z. Jagani, C. Kitidis, H. F. Lodish, R. Khosravi-Far, Cytokines and BCR-ABL mediate suppression of TRAIL-induced apoptosis through inhibition of forkhead FOXO3a transcription factor. *Proc. Natl. Acad. Sci. U.S.A.* **100**, 6523–6528 (2003).
17. J. E. Allen, W. S. El-Deiry, Regulation of the human TRAIL gene. *Cancer Biol. Ther.* **13**, 1143–1151 (2012).
18. F. Bunz, P. M. Hwang, C. Torrance, T. Waldman, Y. Zhang, L. Dillehay, J. Williams, C. Lengauer, K. W. Kinzler, B. Vogelstein, Disruption of p53 in human cancer cells alters the responses to therapeutic agents. *J. Clin. Invest.* **104**, 263–269 (1999).
19. E. L. Greer, A. Brunet, FOXO transcription factors at the interface between longevity and tumor suppression. *Oncogene* **24**, 7410–7425 (2005).
20. J. Y. Yang, C. S. Zong, W. Xia, H. Yamaguchi, Q. Ding, X. Xie, J. Y. Lang, C. C. Lai, C. J. Chang, W. C. Huang, H. Huang, H. P. Kuo, D. F. Lee, L. Y. Li, H. C. Lien, X. Cheng, K. J. Chang, C. D. Hsiao, F. J. Tsai, C. H. Tsai, A. A. Sahin, W. J. Muller, G. B. Mills, D. Yu, G. N. Hortobagyi, M. C. Hung, ERK promotes tumorigenesis by inhibiting FOXO3a via MDM2-mediated degradation. *Nat. Cell Biol.* **10**, 138–148 (2008).
21. T. F. Burns, W. S. El-Deiry, Identification of inhibitors of TRAIL-induced death (ITIDs) in the TRAIL-sensitive colon carcinoma cell line SW480 using a genetic approach. *J. Biol. Chem.* **276**, 37879–37886 (2001).
22. A. Ashkenazi, R. C. Pai, S. Fong, S. Leung, D. A. Lawrence, S. A. Marsters, C. Blackie, L. Chang, A. E. McMurtrey, A. Hebert, L. DeForge, I. L. Koumenis, D. Lewis, L. Harris, J. Bussiere, H. Koeppen, Z. Shahrokh, R. H. Schwall, Safety and antitumor activity of recombinant soluble Apo2 ligand. *J. Clin. Invest.* **104**, 155–162 (1999).
23. V. Modur, R. Nagarajan, B. M. Evers, J. Milbrandt, FOXO proteins regulate tumor necrosis factor-related apoptosis inducing ligand expression. Implications for *PTEN* mutation in prostate cancer. *J. Biol. Chem.* **277**, 47928–47937 (2002).
24. M. C. T. Hu, D. F. Lee, W. Xia, L. S. Golfman, F. Ou-Yang, J. Y. Yang, Y. Zou, S. Bao, N. Hanada, H. Saso, R. Kobayashi, M. C. Hung, IκB kinase promotes tumorigenesis through inhibition of forkhead FOXO3a. *Cell* **117**, 225–237 (2004).
25. N. Finnberg, W. S. El-Deiry, Activating FOXO3a, NF-kappaB and p53 by targeting IKKs: An effective multi-faceted targeting of the tumor-cell phenotype? *Cancer Biol. Ther.* **3**, 614–616 (2004).
26. W. Wang, W. S. El-Deiry, Targeting FOXO kills two birds with one stone. *Chem. Biol.* **11**, 16–18 (2004).
27. W. Yang, N. G. Dolloff, W. S. El-Deiry, ERK and MDM2 prey on FOXO3a. *Nat. Cell Biol.* **10**, 125–126 (2008).
28. V. Desplat, A. Geneste, M. A. Begorre, S. B. Fabre, S. Brajot, S. Massip, D. Thiolat, D. Mossalayi, C. Jarry, J. Guillon, Synthesis of new pyrrolo[1,2-*a*]quinoxaline derivatives as potential inhibitors of Akt kinase. *J. Enzyme Inhib. Med. Chem.* **23**, 648–658 (2008).
29. M. F. Favata, K. Y. Horiuchi, E. J. Manos, A. J. Daulerio, D. A. Stradley, W. S. Feeser, D. E. Van Dyk, W. J. Pitts, R. A. Earl, F. Hobbs, R. A. Copeland, R. L. Magolda, P. A. Scherle, J. M. Trzaskos, Identification of a novel inhibitor of mitogen-activated protein kinase kinase. *J. Biol. Chem.* **273**, 18623–18632 (1998).
30. J. Y. Yang, C. J. Chang, W. Xia, Y. Wang, K. K. Wong, J. A. Engelman, Y. Du, M. Andreeff, G. N. Hortobagyi, M. C. Hung, Activation of FOXO3a is sufficient to reverse mitogen-activated protein/extracellular signal-regulated kinase kinase inhibitor chemoresistance in human cancer. *Cancer Res.* **70**, 4709–4718 (2010).
31. M. M. Shareef, N. Cui, R. Burikhanov, S. Gupta, S. Satishkumar, S. Shajahan, M. Mohiuddin, V. M. Rangnekar, M. M. Ahmed, Role of tumor necrosis factor-α and TRAIL in high-dose radiation–induced bystander signaling in lung adenocarcinoma. *Cancer Res.* **67**, 11811–11820 (2007).
32. H. Walczak, R. E. Miller, K. Ariail, B. Gliniak, T. S. Griffith, M. Kubin, W. Chin, J. Jones, A. Woodward, T. Le, C. Smith, P. Smolak, R. G. Goodwin, C. T. Rauch, J. C. Schuh, D. H. Lynch, Tumoricidal activity of tumor necrosis factor-related apoptosis-inducing ligand in vivo. *Nat. Med.* **5**, 157–163 (1999).
33. A. N. Cornforth, J. S. Davis, E. Khanifar, K. L. Nastiuk, J. J. Krolewski, FOXO3a mediates the androgen-dependent regulation of FLIP and contributes to TRAIL-induced apoptosis of LNCaP cells. *Oncogene* **27**, 4422–4433 (2008).
34. S. J. Park, H. Y. Sohn, J. Yoon, S. I. Park, Down-regulation of FoxO-dependent c-FLIP expression mediates TRAIL-induced apoptosis in activated hepatic stellate cells. *Cell. Signal.* **21**, 1495–1503 (2009).
35. T. R. Kau, F. Schroeder, S. Ramaswamy, C. L. Wojciechowski, J. J. Zhao, T. M. Roberts, J. Clardy, W. R. Sellers, P. A. Silver, A chemical genetic screen identifies inhibitors of regulated nuclear export of a Forkhead transcription factor in PTEN-deficient tumor cells. *Cancer Cell* **4**, 463–476 (2003).
36. H. Ebi, R. B. Corcoran, A. Singh, Z. Chen, Y. Song, E. Lifshits, D. P. Ryan, J. A. Meyerhardt, C. Benes, J. Settleman, K. K. Wong, L. C. Cantley, J. A. Engelman, Receptor tyrosine kinases exert dominant control over PI3K signaling in human *KRAS* mutant colorectal cancers. *J. Clin. Invest.* **121**, 4311–4321 (2011).
37. J. van Grevenynghe, R. A. Cubas, A. Noto, S. DaFonseca, Z. He, Y. Peretz, A. Filali-Mouhim, F. P. Dupuy, F. A. Procopio, N. Chomont, R. S. Balderas, E. A. Said, M. R. Boulassel, C. L. Tremblay, J. P. Routy, R. P. Sékaly, E. K. Haddad, Loss of memory B cells during chronic HIV infection is driven by Foxo3a- and TRAIL-mediated apoptosis. *J. Clin. Invest.* **121**, 3877–3888 (2011).
38. A. Nebbioso, N. Clarke, E. Voltz, E. Germain, C. Ambrosino, P. Bontempo, R. Alvarez, E. M. Schiavone, F. Ferrara, F. Bresciani, A. Weisz, A. R. de Lera, H. Gronemeyer, L. Altucci, Tumor-selective action of HDAC inhibitors involves TRAIL induction in acute myeloid leukemia cells. *Nat. Med.* **11**, 77–84 (2005).
39. J. Abdulghani, W. S. El-Deiry, TRAIL receptor signaling and therapeutics. *Expert Opin. Ther. Targets* **14**, 1091–1108 (2010).
40. S. H. Kim, K. Kim, J. G. Kwagh, D. T. Dicker, M. Herlyn, A. K. Rustgi, Y. Chen, W. S. El-Deiry, Death induction by recombinant native TRAIL and its prevention by a caspase 9 inhibitor in primary human esophageal epithelial cells. *J. Biol. Chem.* **279**, 40044–40052 (2004).
41. W. Wang, S. H. Kim, W. S. El-Deiry, Small-molecule modulators of p53 family signaling and antitumor effects in p53-deficient human colon tumor xenografts. *Proc. Natl. Acad. Sci. U.S.A.* **103**, 11003–11008 (2006).
42. S. Wang, W. S. El-Deiry, Requirement of p53 targets in chemosensitization of colonic carcinoma to death ligand therapy. *Proc. Natl. Acad. Sci. U.S.A.* **100**, 15095–15100 (2003).

43. T. Anastassiadis, S. W. Deacon, K. Devarajan, H. Ma, J. R. Peterson, Comprehensive assay of kinase catalytic activity reveals features of kinase inhibitor selectivity. *Nat. Biotechnol.* **29**, 1039–1045 (2011).
44. K. J. Livak, T. D. Schmittgen, Analysis of relative gene expression data using real-time quantitative PCR and the $2^{-\Delta\Delta CT}$ method. *Methods* **25**, 402–408 (2001).

Acknowledgments: We thank J. Xu for technical assistance, T. Bruggeman and K. Li for their assistance with tissue embedding and processing, T. Fox for his assistance with mass spectrometry, and R. Brucklacher for his assistance with the expression profiling. **Funding:** This work was supported by grants from the NIH and the American Cancer Society (to W.S.E.-D.) and Penn State Hershey Cancer Institute laboratory start-up funds (to W.S.E.-D.). J.E.A. received the 2011 American Association for Cancer Research (AACR)–Bristol-Myers Squibb Oncology Scholar-in-Training Award. W.S.E.-D. is an American Cancer Society Research Professor. **Author contributions:** J.E.A. and W.S.E.-D. designed all the experiments. J.E.A. conducted the experiments and wrote the manuscript. G.S.W. constructed the plasmids used in the high-throughput screening that identified TIC10. G.K. and P.A.M. conducted the high-throughput screening for TRAIL-inducing compounds. J.E.A. and L.P. validated hits from the screen. G.S.W. and J.-Y.Z. made the MDA-MB-231 shTRAIL and control cell lines. J.E.A. and A.S.P. conducted the intracranial xenograft experiments. N.G.D. constructed and validated the myr-Akt HCT116 cell line. E.M. provided freshly resected colon cancer tissue. W.W. constructed the H460 cell line expressing DR5ΔDD-EGFP. K.A.S. assisted with the design and execution of ChIP assays. D.T.D. conducted flow cytometry analysis. W.S.E.-D. supervised the experiments and contributed as senior author including editing of the manuscript and responsibility for oversight of conduct of the research. **Competing interests:** W.S.E.-D. is a co-founder and chief scientific advisor of Oncoceutics Inc., a biotech company focused on developing novel small-molecule anticancer therapies targeting p53-deficient tumors. **Data and materials availability:** We received TIC10 from the NCI Developmental Therapeutics Program. The microarray data for TIC10 have been deposited in the National Center for Biotechnology Information Gene Expression Omnibus database (GSE34194).

Submitted 22 August 2012
Accepted 28 December 2012
Published 6 February 2013
10.1126/scitranslmed.3004828

Citation: J. E. Allen, G. Krigsfeld, P. A. Mayes, L. Patel, D. T. Dicker, A. S. Patel, N. G. Dolloff, E. Messaris, K. A. Scata, W. Wang, J.-Y. Zhou, G. S. Wu, W. S. El-Deiry, Dual inactivation of Akt and ERK by TIC10 signals Foxo3a nuclear translocation, TRAIL gene induction, and potent antitumor effects. *Sci. Transl. Med.* **5**, 171ra17 (2013).

www.sciencetranslationalmedicine.org/cgi/content/full/5/171/171ra17/DC1

Supplementary Materials for

Dual Inactivation of Akt and ERK by TIC10 Signals Foxo3a Nuclear Translocation, TRAIL Gene Induction, and Potent Antitumor Effects

Joshua E. Allen, Gabriel Krigsfeld, Patrick A. Mayes, Luv Patel, David T. Dicker, Akshal S. Patel, Nathan G. Dolloff, Evangelos Messaris, Kimberly A. Scata, Wenge Wang, Jun-Ying Zhou, Gen Sheng Wu, Wafik S. El-Deiry*

*To whom correspondence should be addressed. E-mail: wafik.eldeiry@gmail.com

Published 6 February 2013, *Sci. Transl. Med.* **5**, 171ra17 (2013)
DOI: 10.1126/scitranslmed.3004828

The PDF file includes:

Materials and Methods

RT-PCR. Total RNA was extracted with RNeasy Minikit (Qiagen) by following the manufacturer's instructions. cDNA was generated with SuperScript II (Invitrogen) with 1 µg of RNA and oligo(dT). For qPCR, primers were: TRAIL forward (CAGAGGAAGAAGCAACACATT), TRAIL reverse (GGTTGATGATTCCCAGGAGTTTATTTTG), GAPDH forward (CCACATCGCTCAGACACCAT), GAPDH reverse (GGCAACAATATCCACTTTACCAGAGT). PCR amplification was performed with the Applied Biosystems 7900HT Fast Real-time Detection System. Samples were standardized to 10 ng/µL, and 20 ng of cDNA per sample was then utilized as a template for real-time PCR with SYBR Green Master Mix (Qiagen Corp). Samples were normalized to GAPDH used under identical conditions. For quantitation we used the 2ΔΔCt method of crossing thresholds (*44*) with GAPDH as the endogenous control for normalization. Reactions were performed in 384 well optical plates in a 7900HT instrument (Applied Biosystems), with 10 µL reaction volumes. Data were analyzed with ABI PRISM 7900 Sequence Detection System 2.2 software. To exclude the possibility of genomic DNA contamination, control PCR reactions with no cDNA template and no-RT control samples were also performed for each gene-specific primer set. Each PCR reaction was performed in quadruplicate and the resulting data were averaged. Semi-quantitative PCR primers were: ERK forward (ACAGGCTGTTCCCAAATGCT), ERK reverse (CCTCCCTTGCTAGAGCTCACT), GAPDH forward (TCTCCCCTTCCTGCAGACAGCTC), GAPDH reverse (TGTGCGGAACCGCTGACACAG). cDNA was amplified with FastStart Taq DNA polymerase (Roche) according to manufacturer's protocols.

Immunofluorescence. Cells were fixed and permeabilized with Cytofix/Cytoperm solution (BD Biosciences). Cells were incubated with anti-active caspase-3 (559565, BD Pharmingen) at 1:250 in Perm/Wash solution (BD Biosciences) for 1 hour in the absence of light. Anti-rabbit Alexa Fluor 488 was incubated at 1:200 in Perm/Wash solution for 20 min at room temperature and rinsed in PBS. Hoechst 33342 (Invitrogen) was used as a nuclear counterstain according to the manufacturer's protocol.

Co-cultures. Co-cultures of HCT116 p53-/- and HFF cells were performed in a 1:1 mixture of complete DMEM and McCoy's 5A medium (Thermo Fisher Scientific Inc.). For fluorescence images, the two cell types were separately labeled with Fluorescent Cell Linkers Kits for general cell membrane labeling (Sigma) according to the manufacturer's protocols. Cells were counterstained with Hoechst 33342 as described in the immunofluorescence section. For flow cytometry analysis of cell death, the two populations of cells were identified by differential light scattering and analyzed as described for sub-G1 analysis in the cell death assays section.

Mass spectrometry

Samples were analyzed on an Acquity Ultra Performance Liquid Chromatography (UPLC) system coupled to a Waters SYNAPT qTOF mass spectrometer. The column, which was kept at 40℃, was a Waters UPLC C18 2.1×50 mm with 1.7 µm particles. The binary solvent system included (A) water containing 0.1% formic acid and 10 mM ammonium formate and (B) acetonitrile containing 0.1% formic acid. The column had a linear gradient that went from 10% A to 50% B. The total run time, including re-equilibration, was 8 min. with a flow rate of 0.200 ml/min. The temperature of the sample organizer was set at 8℃. Approximately 2 pmol of compound was injected. The compound was analyzed by electrospray ionization in positive ion mode. The data were collected at mass range of m/z 50–1000 with scan duration of 0.2 sec. The source temperature was set at 120℃ and nitrogen was used as desolvation gas (700 L/h) at 400℃. The voltages of the sampling cone and capillary were 35 V and 3.5 kV, respectively. Leukine Enkephalin was used as the lockspray reference compound (10 µL/min; 10 sec scan frequency). Tandem mass spectrometry was used for the generation of fragment ions. MS/MS was performed with a collision energy ramp from 20 to 50 V. Elemental composition and assignment of structures to observed fragment ions were performed with MarkerLynx software. For metabolic analysis, 1 mL fractions corresponding to a retention time of 8.5-9.5 minutes were collected from HPLC with the HPLC-based assay for TIC10 as described below for the pharmacokinetic analysis of TIC10. Reanalyzing fraction samples by HPLC validated the accuracy of fraction collection. Samples were speed vacuumed and resuspended in 200 µL of 95% methanol and 5% dH_2O for metabolic analysis.

In vivo studies. All intraperitoneal and intravenous injections were given at a total volume of 200 µL. Oral formulations of TIC10 were administered by oral gavage and given as a 200 µL suspension containing 20% Cremophor EL (Sigma), 10% DMSO, and 70% PBS. Tumors were monitored with digital calipers at indicated time points. All subcutaneous tumors were allowed to establish for 1-4 weeks post-injection until reaching a volume of ~125 mm^3 before treatment initiation. Relief of tumor burden was monitored for 3 weeks after disappearance of the tumor and confirmed by visual inspection after euthanasia. For intracranial xenografts, anesthetized athymic nude mice were implanted with 2 x 10^5 SF767 cells in a 25 µL suspension of serum- and antibiotic-free RPMI (Thermo Fisher Scientific Inc.). The site of injection was a burr hole created 1 mm lateral to the midline of the skull and 1 mm anterior to the coronal suture. The injection was gradually administered over 5 minutes with a Hamilton syringe, and the burr hole was sealed with bone wax. Tumor take was assessed by bioluminescent imaging 2 weeks after implantation. Bioluminescent imaging of tumors was carried out on an IVIS imaging system as previously described (42). Near-infrared imaging of mice was carried out on a Pearl Impulse imaging system (LI-COR) after tail-vein injection of Angiosense 680 (VisEn Medical) according to the manufacturer's protocols. 6 week old Eµ-myc mice were obtained from The Jackson Laboratory (B6.Cg-Tg(IghMyc)22Bri/J). For serum chemistry assays, 1 mL of blood was harvested from anesthetized mice by terminal cardiac puncture of the left ventricle.

Blood was placed into a microfuge tube and allowed to clot for 30 minutes at room temperature, then centrifuged. Serum was removed and centrifuged again to remove any further clots, then submitted for analysis.

Pharmacokinetic analysis of TIC10. HPLC analysis was performed by absorbance detection at 239 nm on an Agilent 1200 series system with an Eclipse XDB –C18 column (Agilent) and a 100 µL injection loop. Isocratic elution at 1 mL/minute was carried out in 0.1% trifluoroacetic acid in deionized distilled H_2O. An acetonitrile (ACN) gradient was carried out for elution as 15-20% ACN for 0-5 minutes, 20-23% for 5-12 minutes, 25% for 12-18 minutes. The standard curve was generated by spiking varying concentrations of TIC10 into plasma harvested from athymic nude mice from unrelated experiments. For all plasma samples, blood was obtained by terminal cardiac puncture of the left ventricle and collected into EDTA tubes (BD). Samples were centrifuged at 500 g for 10 minutes. Plasma was deproteinated by adding 30 µL of perchloric acid to 100 µL of samples, vortexing for 15 seconds, centrifugation for 2 minutes, and immediately injecting the supernatant into the HPLC. AUC was normalized to an internal serum peak with a retention time of 8.1 minutes. AUC data versus time was fit with a two-compartment open model, assuming first order elimination from central compartment with the equation $AUC = Ae^{-\alpha t} + Be^{-\beta t}$, where t = time, and A and B are the extrapolated concentrations at the initiation of the two phases (distribution and elimination). Half-lives were calculated as $t_{1/2\alpha}=0.693/\alpha$ and $t_{1/2\beta}=0.693/\beta$. Other equations used for calculation included $CL=dose/AUC_{0-\infty}$ and $V_d=dose/(AUC_{0-\infty} X \beta)$.

Tissue analyses. Mice were humanely sacrificed by cervical dislocation under anesthesia at indicated time points, and excised normal tissue or tumors were fixed in 4% paraformaldehyde in PBS overnight at 4℃. For RT-qPCR and Western blot analysis, tumors were minced and homogenized in lysis buffer and then prepared as described for such analyses in cell culture. Paraffin-embedding, serial sectioning of slides, and hematoxylin and eosin staining were carried out by the Penn State Hershey Histology Core Facility. TUNEL staining was performed with the ApopTag Peroxidase In Situ Apoptosis Detection Kit (Millipore). For IHC analysis, slides were dewaxed in xylene and hydrated in a decreasing gradient of ethanol. Antigen retrieval was carried out by boiling in 10 mM citric acid (pH 6.0) for 6 minutes. Samples were blocked with streptavidin and biotin blocking solutions and goat serum (Vector Laboratories). Primary antibodies were incubated overnight at 4℃ in a humidity chamber. Incubation with biotinylated secondary antibody and DAB deposition was carried out according to the manufacturer's protocol (Vector Laboratories DAB Substrate Kit for Peroxidase). Samples were counterstained with hematoxylin (DAKO) for 6 min, rinsed in dH_2O for 5 min, rinsed with PBS, and dehydrated and sealed under cover slips. Images were recorded on an Axioskop microscope with QCapture software (QImaging).

In vitro kinase assays. In vitro kinase assays were conducted by Reaction Biology Corporation as previously described (*43*).

Gene expression analysis. HCT116 $p53^{-/-}$ cells were grown in log-phase and treated with DMSO or TIC10 (10 μM). At 48 hours, total RNA was isolated with the RNeasy Mini Kit (Qiagen). Microarray analysis was performed with the Illumina HT-12 Beadchip in the Penn State University College of Medicine Genome Sciences Facility. RNA quality and concentration was assessed with an Agilent 2100 Bioanalyzer with RNA Nano LabChip. cRNA was synthesized by TotalPrep Amplification (Ambion) from 500 ng of RNA according to manufacturer's instructions. T7-oligo(dT) primed reverse transcription was used to produce first strand cDNA. cDNA then underwent second strand synthesis and RNA degradation by DNA Polymerase and RNase H, followed by filtration clean up. *In vitro* transcription (IVT) was employed to generate multiple copies of biotinylated cRNA. The labeled cRNA was purified by filtration, quantified by NanoDrop, and volume-adjusted for a total of 750 ng/sample. Samples were fragmented and denatured before hybridization for 18 hours at 58°C. After hybridization, beadchips were washed and fluorescently labeled. Beadchips were scanned with a BeadArray Reader (Illumina). A project was created with the resultant scan data and imported into GenomeStudio 1.0 (Illumina). Results were exported to GeneSpring Gx11 (Agilent Technologies). Measurements less than 0.01 were then set to 0.01, arrays normalized to the 50^{th} percentile, and individual genes normalized to the median of controls. For network analysis of transcriptional changes induced by TIC10, the dataset was analyzed with the Ingenuity Pathway Analysis software. Microarray data have been deposited into the NCBI GEO database (http://www.ncbi.nlm.nih.gov/geo/query/acc.cgi?token=ppihbcummescwji&acc=GSE34194).

Plasmids. WT (Plasmid #1787) and DB (Plasmid #8354) Foxo3a constructs were obtained through Addgene and transfected at 4 μg per $5X10^6$ cells with Oligofectamine 2000 (Invitrogen).

Supplementary Figures

Figure S1

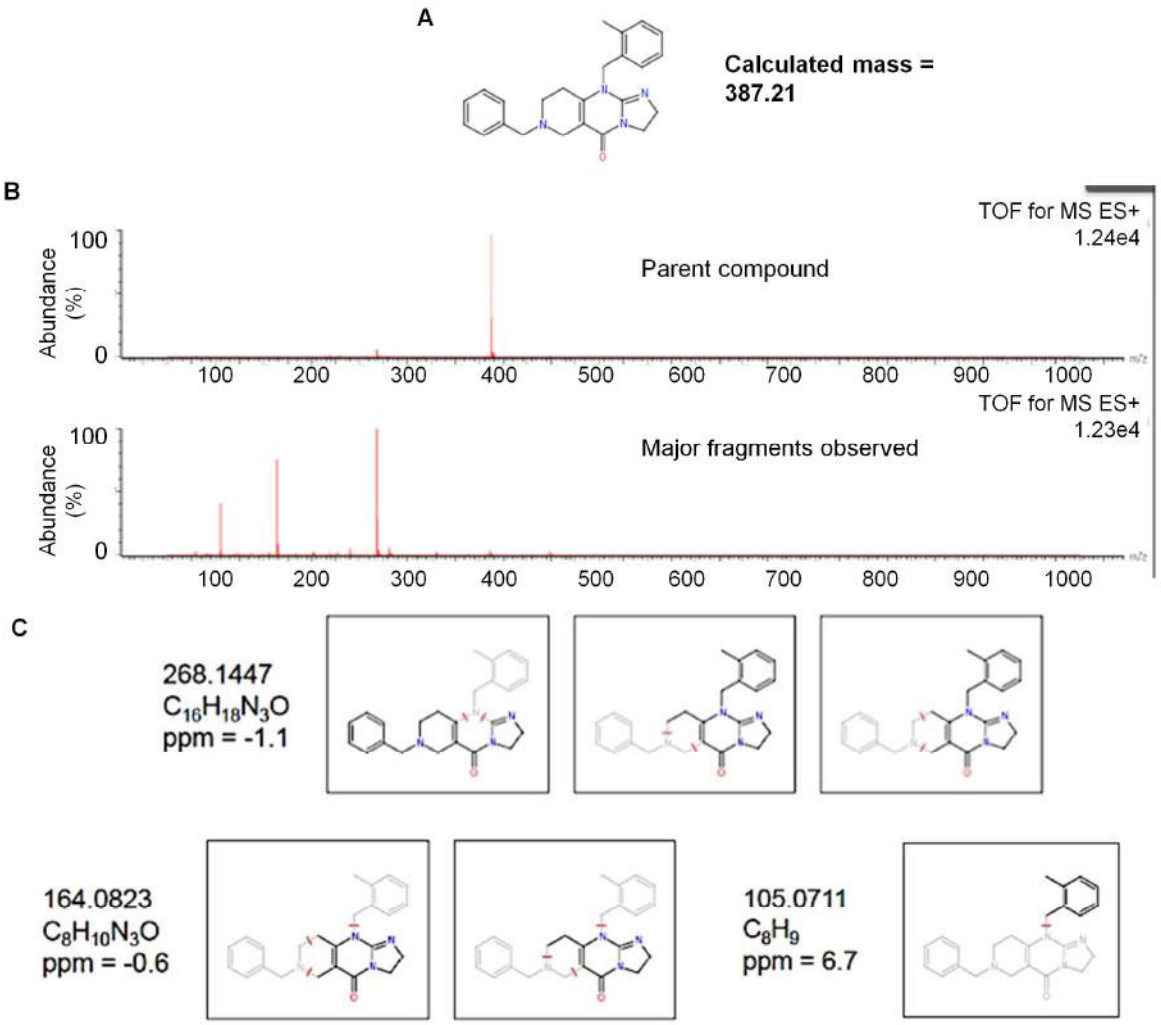

Figure S1. TIC10 structure was confirmed by mass spectrometry. (A) Predicted structure and mass of TIC10. (B) Mass spectrometry analysis of TIC10 showing the parent compound (top panel) and major fragments (bottom panel) (C) Potential structures of major fragments correspond with the predicted structure of TIC10.

Figure S2

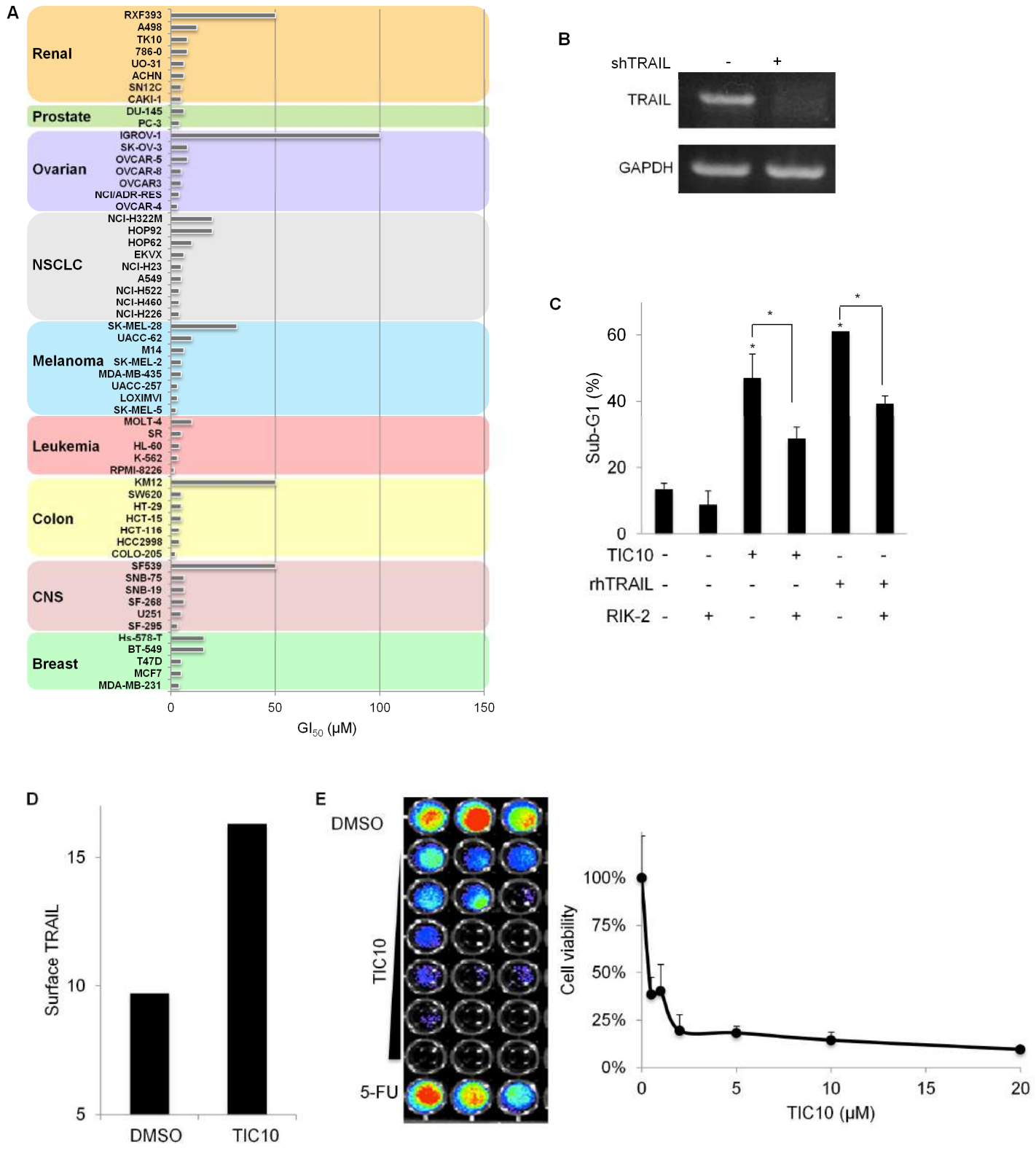

Figure S2. TIC10 exhibits broad-spectrum and TRAIL-specific activity in vitro. (A) GI_{50} for TIC10 data across the NCI60 cell lines. (B) Verification of MDA-MB-231 shTRAIL knockdown at the mRNA level by RT-PCR analysis. (C) Percentage of sub-G1 DNA in HCT116 cells treated with DMSO, TIC10 (10 μM), or rhTRAIL (25 ng/mL) in the presence or absence of a TRAIL-sequestering antibody, RIK-2 (72 hours, *n* = 3). (D) TIC10-induced surface TRAIL in freshly

resected colon cancer cells (10 μM, 72 hours). Data are expressed as median fluorescence intensity. (E) Cell viability assay of primary colon cancer cells from (D) treated with DMSO, TIC10 (0.6, 1.25, 2.5, 5, 10, and 20 μM from top to bottom), or 5-FU (5 μM) (n = 3). Error bars indicate s.d. of replicates. *P < 0.05 compared to control unless otherwise indicated.

Figure S3

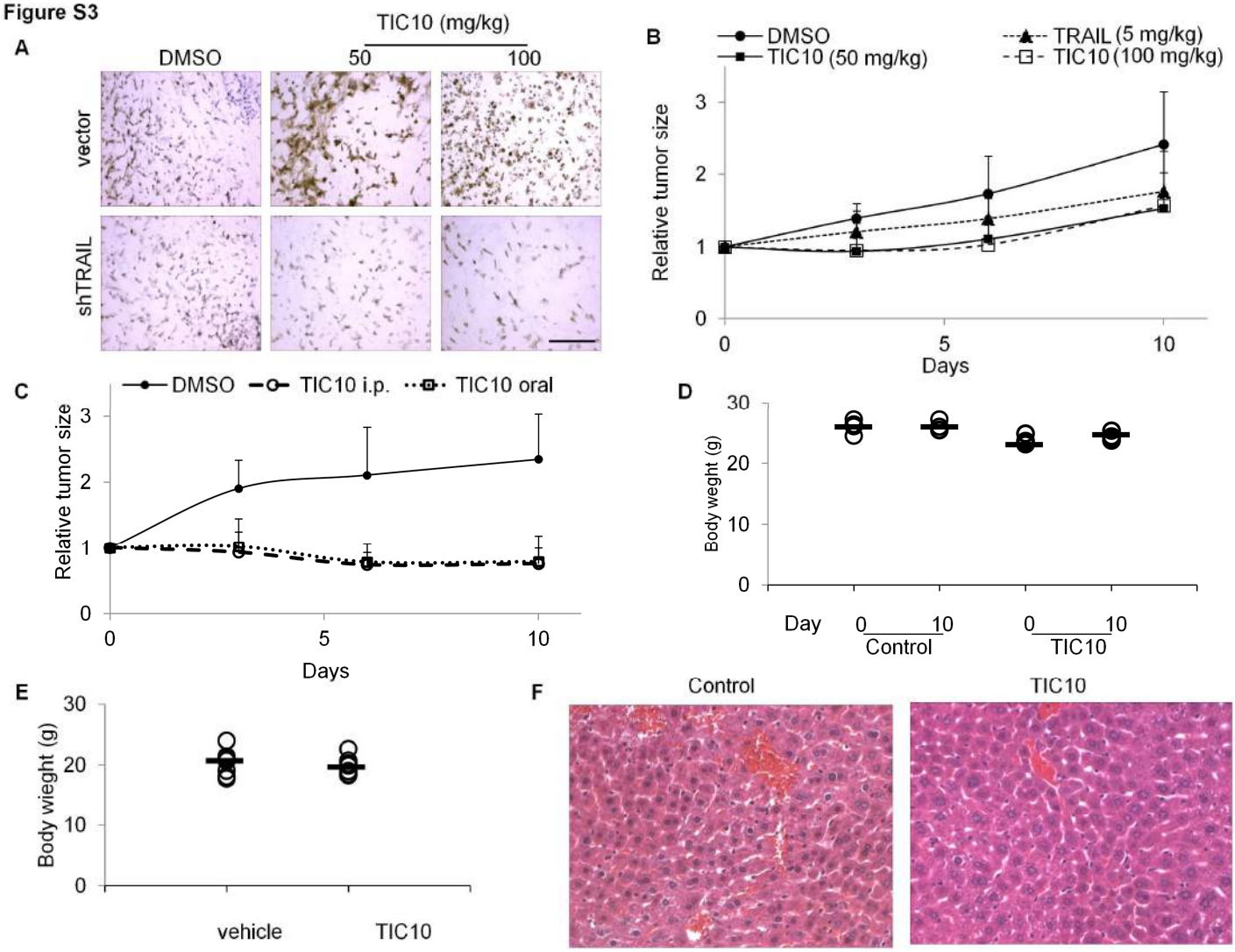

Figure S3. TIC10 induces TRAIL-mediated apoptosis and is nontoxic in vivo. (A) TUNEL staining of MDA-MB-231 xenograft tumors expressing vector and shTRAIL 2 days after treatment with TIC10. (B) Relative tumor volume (compared to day 0) of DLD-1 xenografts treated with TRAIL (i.v.), TIC10 (i.p.), or DMSO (i.p.) as a single dose on day 0 at indicated concentrations (*n* = 8). (C) Comparison of i.p. versus oral administration of a single dose of TIC10 at 30 mg/kg in SW480 xenografts treated on day 0 (*n* = 6). (D) Body weight of athymic female nude mice treated with a single dose of TIC10 (100 mg/kg, i.p.) (*n* = 4). (E) Body weight of C57/B6 female mice at the end of week 4 of treatment with a single weekly dose of oral TIC10 (25 mg/kg) for 4 weeks (*n* = 5). (F) H&E staining of liver from athymic female nude mice harvested 3 days after treatment with TIC10 (100 mg/kg, i.p.) or DMSO control. Scale bars are 100 μm. Error bars indicate s.d. of replicates.

Figure S4

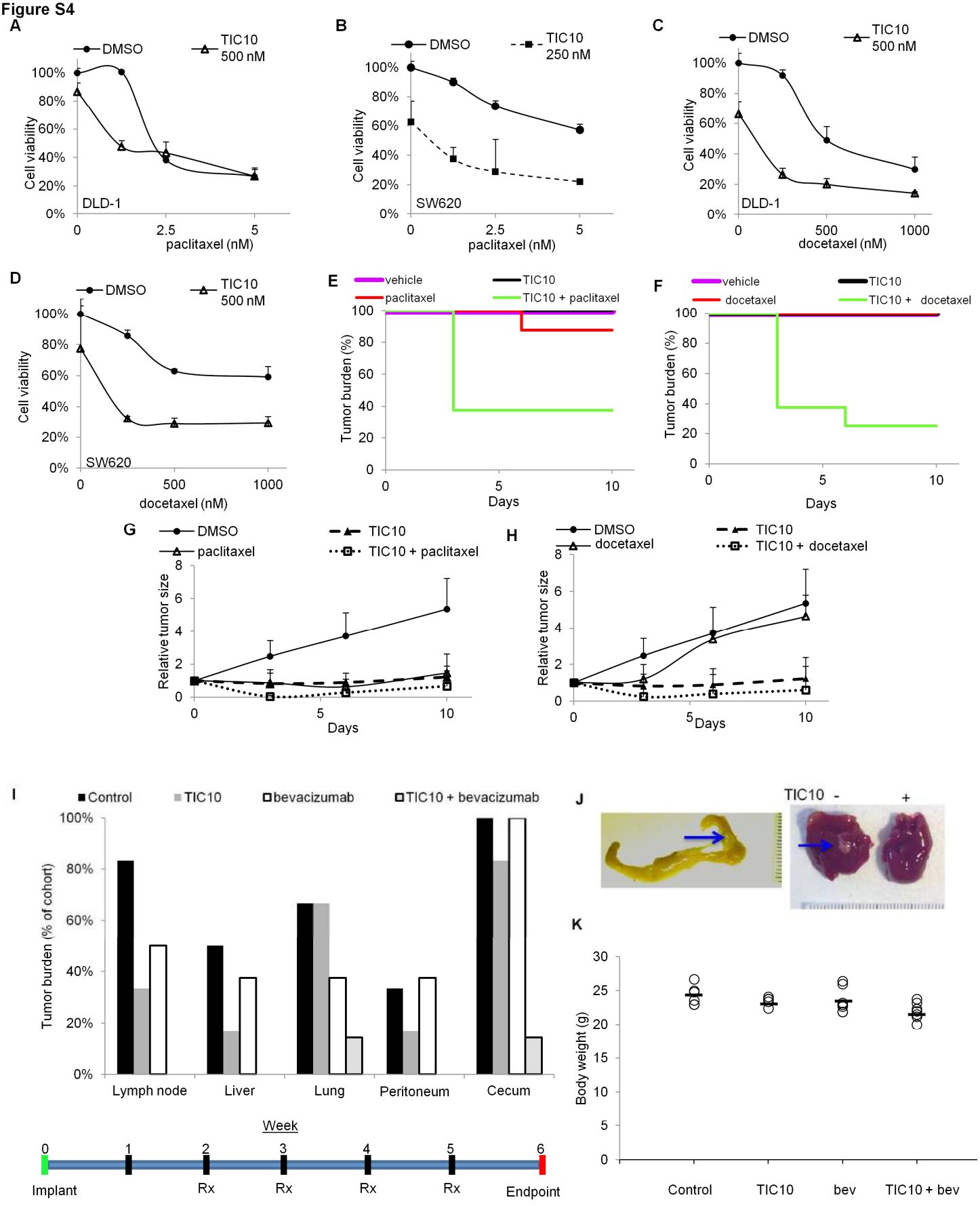
A
DMSO
TIC10 500 nM
Cell viability
DLD-1
paclitaxel (nM)
B
DMSO
TIC10 250 nM
SW620
paclitaxel (nM)
C
DMSO
TIC10 500 nM
DLD-1
docetaxel (nM)
D
DMSO
TIC10 500 nM
SW620
docetaxel (nM)
E
vehicle
TIC10
paclitaxel
TIC10 + paclitaxel
Tumor burden (%)
Days
F
vehicle
TIC10
docetaxel
TIC10 + docetaxel
Tumor burden (%)
Days
G
DMSO
TIC10
paclitaxel
TIC10 + paclitaxel
Relative tumor size
Days
H
DMSO
TIC10
docetaxel
TIC10 + docetaxel
Relative tumor size
Days
I
Control
TIC10
bevacizumab
TIC10 + bevacizumab
Tumor burden (% of cohort)
Lymph node
Liver
Lung
Peritoneum
Cecum
Week
Implant
Rx
Endpoint
J
TIC10 - +
K
Body weight (g)
Control
TIC10
bev
TIC10 + bev

Figure S4. TIC10 cooperates with taxanes and bevacizumab. Cell viability of (A) DLD-1 and (B) SW620 cells treated with TIC10 in combination with paclitaxel at indicated concentrations (72 hours, *n* = 3). Cell viability of (C) DLD-1 and (D) SW620 cells treated with TIC10 in combination with docetaxel at indicated conditions (72 hours, *n* = 3). (E) Percent of each cohort in mice bearing H460 xenografts that retain tumor burden after treatment with TIC10 (30 mg/kg, i.p.) and/or paclitaxel (20 mg/kg, i.v.) or with vehicle (DMSO, i.p.) (*n* = 8) as single doses. (F) Percent of each cohort of mice bearing H460 xenografts that retain tumor burden after treatment with TIC10 (30 mg/kg, i.p.) and/or docetaxel (20 mg/kg, i.v.) or with vehicle (DMSO, i.p.) (*n* = 8) as single doses. (G) and (H) are the relative tumor volume plots for (E) and (F), respectively. Tumor volumes are normalized to the volumes at day 0. (I) Percent of each cohort implanted with intracecal HCT116 $p53^{-/-}$ cells that have detectable tumor at the primary and distal sites at the 6-week endpoint (*n* = 5). As indicated by the time line, treatment was administered once a week starting at 2 weeks post-implantation, with cohorts receiving vehicle, TIC10 (25 mg/kg, oral), bevacizumab (bev, 10 mg/kg, i.v.), or the combination of TIC10 and bevacizumab. (J) Images of sample tumors (marked with arrows) in the cecum (left panel) and liver at week 6 post-implantation. Right panel shows an apparent liver metastasis in a vehicle-treated mouse. (K) Body weight of mice at the endpoint. Error bars indicate s.d. of replicates.

Figure S5

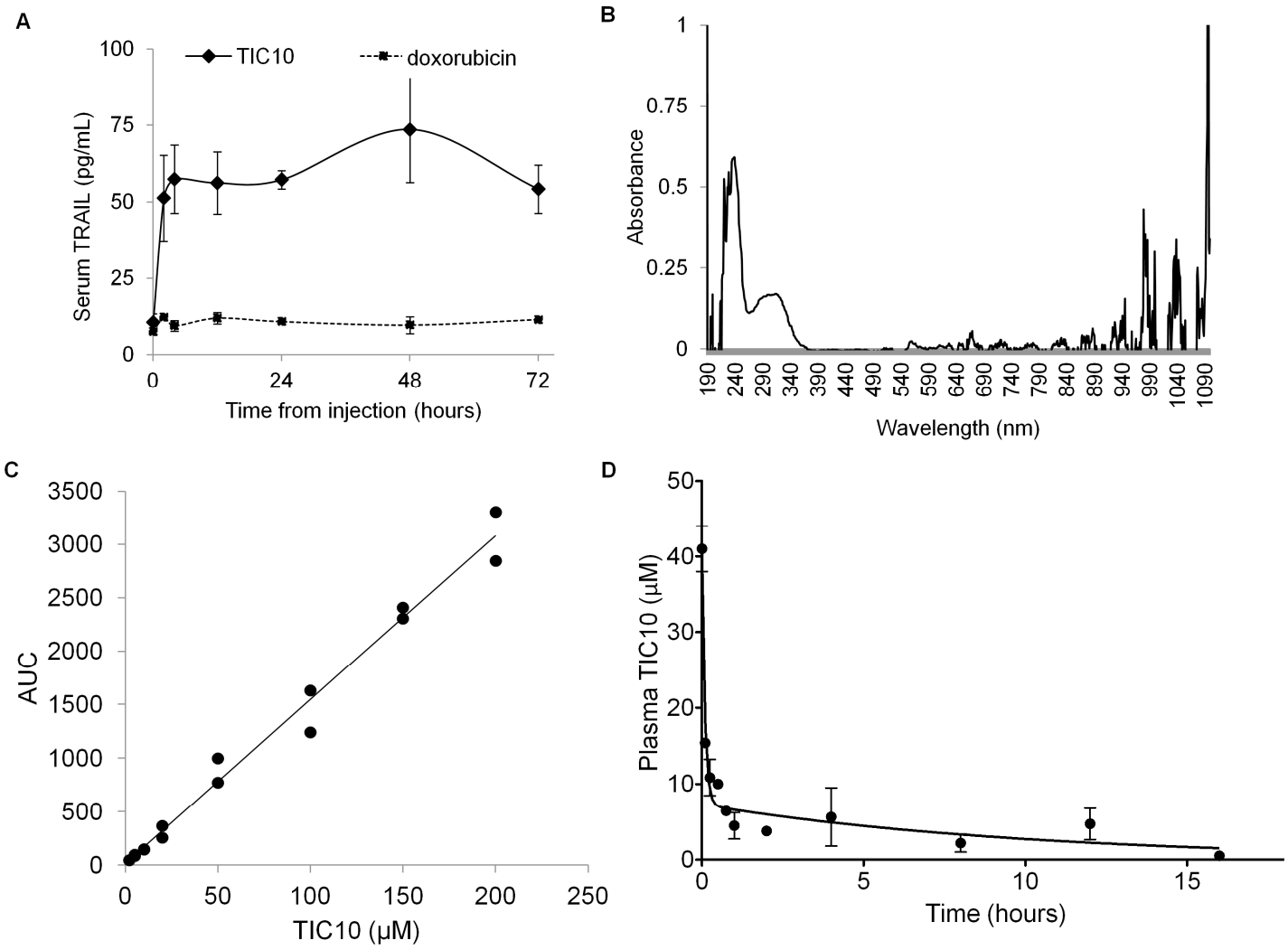

Figure S5. The pharmacokinetics of TIC10 were analyzed in tumor-free mice. (A) TRAIL serum levels in tumor-free mice after injection of TIC10 (100 mg/kg, i.v.) or doxorubicin (30 mg/kg, i.p.) (*n* = 2). (B) Absorbance profile of TIC10 with a peak absorbance at 239 nm. (C) Calibration curve for TIC10 spiked into mouse plasma and quantitated by HPLC analysis to calculate area under curve (AUC). (D) Plasma concentrations of TIC10 after intravenous administration at 25 mg/kg in C57/B6 female mice (*n* = 3). Error bars represent standard error of replicates.

Figure S6

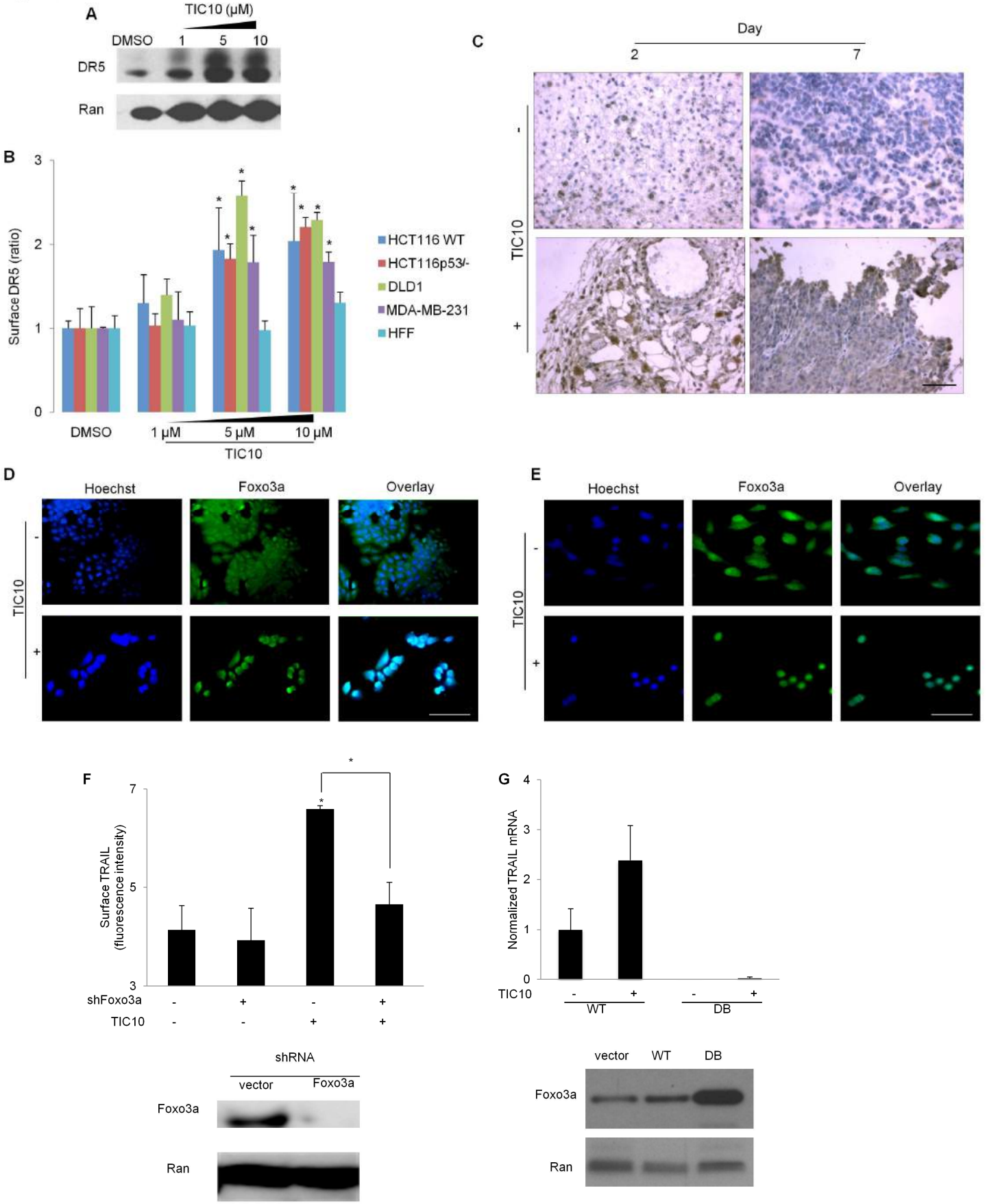
A
TIC10 (μM)
DMSO
1
5
10
DR5
Ran
B
Surface DR5 (ratio)
HCT116 WT
HCT116p53-/-
DLD1
MDA-MB-231
HFF
DMSO
1 μM
5 μM
10 μM
TIC10
C
Day
2
7
TIC10
D
Hoechst
Foxo3a
Overlay
TIC10
E
Hoechst
Foxo3a
Overlay
TIC10
F
Surface TRAIL (fluorescence intensity)
shFoxo3a
TIC10
shRNA
vector
Foxo3a
Foxo3a
Ran
G
Normalized TRAIL mRNA
TIC10
WT
DB
vector
WT
DB
Foxo3a
Ran

Figure S6. TIC10 up-regulates DR5 and induces Foxo3a activity by stimulating nuclear translocation. (A) Western blot analysis of DR5 in HCT116 cells treated with TIC10 or DMSO at indicated concentrations for 72 hours. Ran shown as a loading control. (B) Flow cytometry analysis of surface DR5 in cancer and normal cells treated with TIC10 (72 hours, *n* = 3). (C) IHC analysis of DR5 expression in HCT116 xenograft tumors treated with vehicle (DMSO, i.p.) or TIC10 (100 mg/kg, i.p.). Immunofluorescence of Foxo3a in (D) H460 and (E) SW480 cells treated with DMSO or TIC10 (10 μM, 48 hours). Foxo3a is shown in green and Hoechst 33342 is shown in blue as a nuclear counterstain. (F) Flow cytometry analysis of TIC10-induced surface TRAIL with or without stable knockdown of Foxo3a in HCT116 cells (10 M, 72 hours, *n* = 3). Confirmation of Foxo3a stable knockdown by Western blot analysis shown below. (G) RT-qPCR analysis of TRAIL messenger-RNA in HCT116 cells transfected with wild-type Foxo3a (WT) or Foxo3a lacking its DNA binding domain (DB) and treated with DMSO or TIC10 (5 μM, 48 hours, *n* = 4), normalized to WT samples without TIC10. Western blot analysis of Foxo3a construct expression shown below. Scale bars are 100 μm and apply to all figures within a panel. Error bars indicate s.d. of replicates. *$P < 0.05$ compared to control unless otherwise indicated.

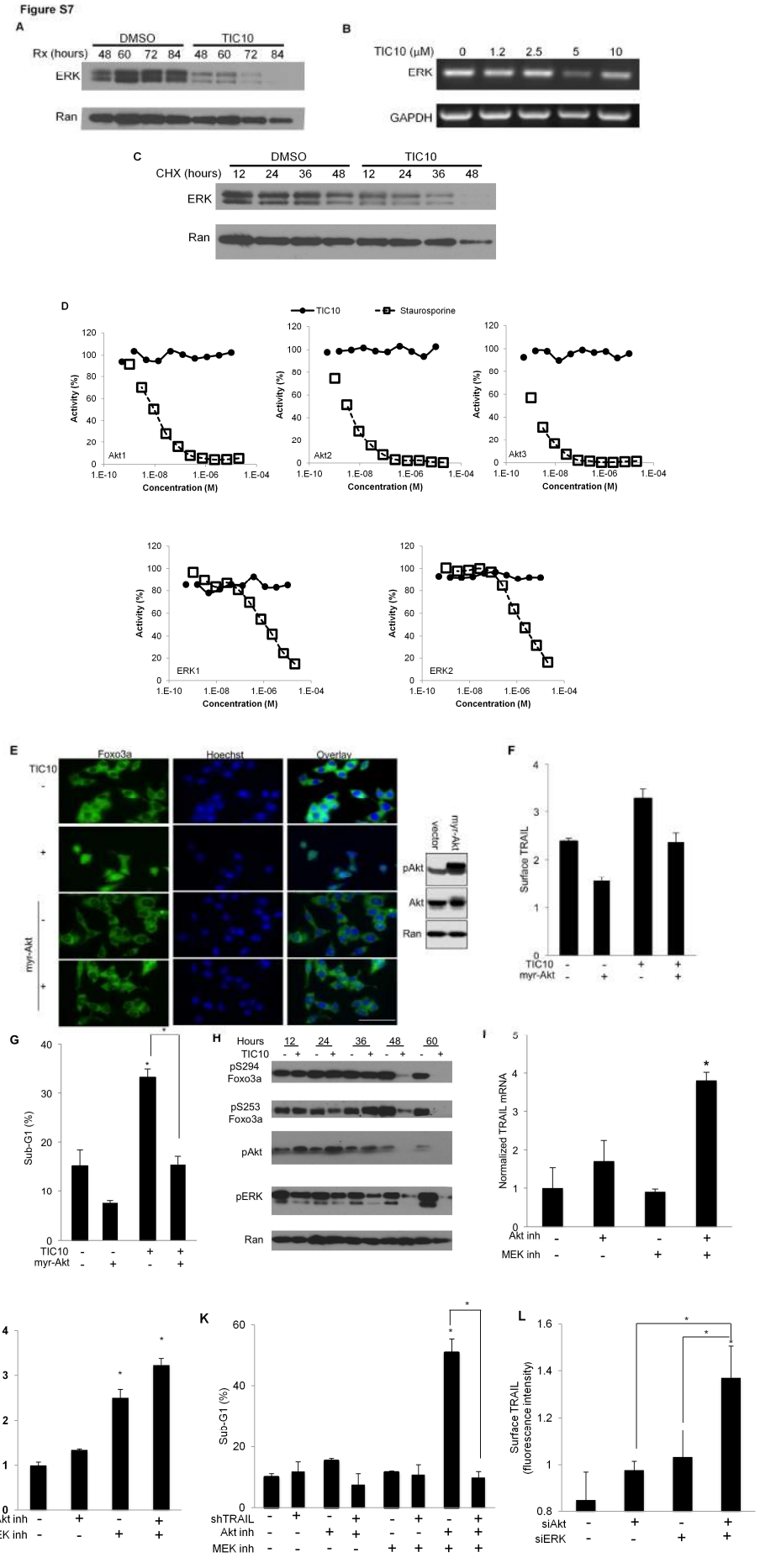
Figure S7
A
DMSO
TIC10
Rx (hours) 48 60 72 84 48 60 72 84
ERK
Ran
B
TIC10 (μM) 0 1.2 2.5 5 10
ERK
GAPDH
C
DMSO
TIC10
CHX (hours) 12 24 36 48 12 24 36 48
ERK
Ran
D
TIC10
Staurosporine
Activity (%)
Akt1
Akt2
Akt3
ERK1
ERK2
Concentration (M)
E
Foxo3a
Hoechst
Overlay
TIC10
myr-Akt
vector
pAkt
Akt
Ran
F
Surface TRAIL
TIC10
myr-Akt
G
Sub-G1 (%)
TIC10
myr-Akt
H
Hours 12 24 36 48 60
TIC10
pS294 Foxo3a
pS253 Foxo3a
pAkt
pERK
Ran
I
Normalized TRAIL mRNA
Akt inh
MEK inh
J
Surface TRAIL (ratio)
Akt inh
MEK inh
K
Sub-G1 (%)
shTRAIL
Akt inh
MEK inh
L
Surface TRAIL (fluorescence intensity)
siAkt
siERK

Figure S7. Akt and ERK are indirectly inhibited by TIC10 and affect TIC10-induced TRAIL signaling and cell death. (A) Western blot analysis of ERK expression after TIC10 treatment in HCT116 cells for the indicated number of hours (5 μM). (B) RT-PCR analysis of ERK mRNA in HCT116 cells after TIC10 treatment at indicated concentrations (48 hours). (C) Western blot analysis of ERK expression in HCT116 cells treated with TIC10 (5 μM, 48hr), then with cycloheximide (CHX; 10 μM) for the indicated number of hours. (D) Kinase activity assays for TIC10 inhibition of Akt and ERK isoforms with staurosporine as a positive control. (E) Immunofluorescence of Foxo3a in HCT116 cells overexpressing myristoylated Akt (myr-Akt) with and without TIC10 treatment (10 μM, 48 hours). Confirmation of overexpression of myr-Akt by Western blot shown in right panel. Scale bar is 100 μm and applies to all images within the panel. (F) Flow cytometry analysis of surface TRAIL and (G) Percentage of sub-G1 DNA in HCT116 cells overexpressing an empty vector or myr-Akt with and without TIC10 treatment (10 μM, 72 hours, $n = 3$). (H) Time course Western blot analysis of HCT116 $p53^{-/-}$ cells treated with DMSO or TIC10 (5 μM) for indicated time periods. (I) RT-qPCR analysis of TRAIL mRNA in HCT116 $p53^{-/-}$ cells after incubation with 10 μM A6730 (Akt inhibitor), 10 μM U0126 monoethanolate (MEK inhibitor), or both (48 hours, $n = 3$). Data are normalized to GAPD mRNA concentration. (J) Surface TRAIL analysis of HCT116 $p53^{-/-}$ cells after incubation with 10 μM A6730 (Akt inh), 10 μM U0126 monoethanolate (MEK inh), or both (48 hours, $n = 3$), normalized to untreated cells. (K) Percentage of sub-G1 DNA in MDA-MB-231 with or without TRAIL knockdown by shRNA after incubation with 10 μM Akt inhibitor, MEK inhibitor, or both for 48 hours ($n = 3$). (L) Surface TRAIL analysis at 48 hours after transient knockdown of Akt and/or ERK in HCT116 cells ($n = 3$). $^*P < 0.05$ compared to control unless otherwise indicated.

Figure S8

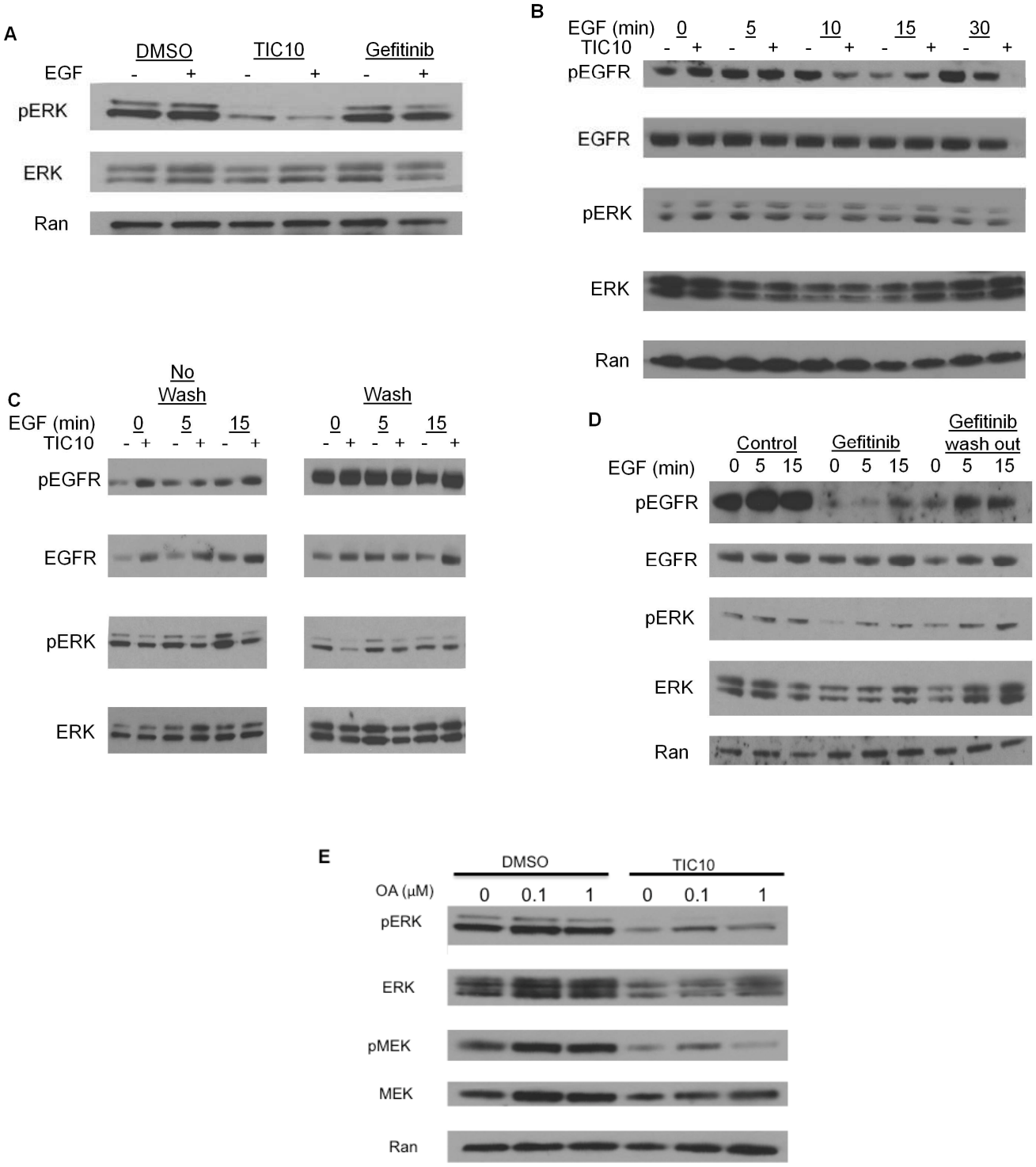

Figure S8. TIC10 indirectly inhibits the MAPK pathway downstream of EGFR. (A) Western blot analysis of pERK in HCT116 cells treated with DMSO, TIC10 (5 μM), or gefitinib (5 μM) (48 hours) and then stimulated with EGF (100 ng/mL) for 15 minutes. (B) Time course Western blot analysis of HCT116 cells treated with TIC10 (5 μM, 48 hours) and then stimulated with EGF (100 ng/mL) for the indicated time. (C) Western blot analysis of EGFR and ERK expression and phosphorylation in HCT116 cells treated with TIC10 (5 μM, 48 hours), followed by replacing the medium with complete

medium containing EGF (100 ng/mL) with (no wash) or without (wash) TIC10 for the indicated time. (D) The same analysis as in (C) but with gefitinib (5 μM). (E) Western blot analysis of pERK in HCT116 cells treated with TIC10 (5 μM, 48 hours) in the presence or absence of okadaic acid (OA).

Table S1. The serum chemistry of C57/B6 mice treated with TIC10 (25 mg/kg) weekly for 4 weeks was unchanged compared to vehicle-treated mice (*n* = 3).

Cohort	Sodium (mM)	Potassium (mM)	Chloride (mM)	Total bilirubin (mg/dl)	Blood urea nitrogen (mg/dl)	Creatinine (mg/dl)	Total Protein (g/dl)	Albumin (g/dl)	Alkaline phosphate (U/L)	Lactate dehydrogenase (U/L)
Control	151.5±4.2	9.025±2.2	106.75±1.7	3.075±1.6	26±1.6	0.25±.06	4.9±.36	3±.08	104.5	265
TIC10	154.5±5.2	7.325±3.2	104	2.725±2.4	33.75±7.3	0.15±.06	4.97±.61	2.9	112±12	287.5±125

Table S2. TIC10 metabolites in vitro varied over time. HCT116 $p53^{-/-}$ cells were treated with TIC10 (10 μM) for the indicated time period. Supernatants were subjected to mass spectrometry analysis. Peaks showing a time-dependent relationship are highlighted in yellow. Prevalent potential metabolites are highlighted in light blue. R.T. is the retention time on the HPLC column.

Peak ID	Name	m/z	R.T. (min)	MS Area 0hours	MS Area 12hours	MS Area 24hours	MS Area 36hours	MS Area 48hours	MS Area 60hours	MS Area 72hours
C1	Demethylation and Methylene to Ketone	387.1939	9.62	1.00E+03	1.81E+03	1.19E+03			1.42E+03	1.73E+03
C2	Desaturation	385.202	10.62					1.49E+03		
C3	Gain of 0.1311	387.349	12.15		7.79E+02					
C4	Gain of 1.0377	388.2556	4.98					2.26E+04		
C5	Gain of 10.0553	397.2732	11.85		2.99E+03	3.75E+03	4.06E+03		2.49E+03	1.16E+03
C6	Gain of 10.0752	397.2931	10.76	1.97E+03						
C7	Gain of 101.1407	488.3587	10.57					1.35E+03		
C8	Gain of 106.2808	493.4988	12.99	8.62E+03						
C9	Gain of 115.1571	502.375	10.89	1.16E+03						
C10	Gain of 118.2817	505.4996	12.91						2.98E+03	
C11	Gain of 12.0180	399.2359	6.98	1.31E+03						
C12	Gain of 12.0343	399.2522	10.5				1.91E+03	6.71E+03		
C13	Gain of 120.1120	507.3299	10.89	7.32E+03	5.83E+03	5.47E+03	6.06E+03		4.66E+03	4.26E+03

C14	Gain of 120.2963	507.5142	13.34	4.95E+03						
C15	Gain of 122.1382	509.3562	8.31					1.02E+03		
C16	Gain of 123.9403	511.1583	9.54					6.31E+03		
C17	Gain of 123.9412	511.1591	9.29				9.21E+03	3.55E+04		
C18	Gain of 129.2113	516.4292	12.59	2.86E+03		4.70E+03				5.04E+03
C19	Gain of 13.1611	400.379	12.36							3.05E+03
C20	Gain of 13.1628	400.3807	12.9	1.18E+03						
C21	Gain of 134.0919	521.3098	11.84					9.61E+04		
C22	Gain of 146.3124	533.5304	13.49						4.44E+03	
C23	Gain of 146.3150	533.533	13.49			3.13E+03				
C24	Gain of 159.1834	546.4013	10.91			4.81E+03				
C25	Gain of 161.2862	548.5041	13.32				4.69E+04			
C26	Gain of 163.3397	550.5577	13.49		3.21E+03					
C27	Gain of 163.4111	550.6291	12.88			2.74E+03				
C28	Gain of 163.4116	550.6296	13.36				2.65E+04			
C29	Gain of 164.2855	551.5034	13.29		1.52E+03				1.55E+03	1.27E+03
C30	Gain of 168.2941	555.5121	13.46		5.10E+03					
C31	Gain of 17.1212	404.3392	11.93		1.33E+03	5.24E+03	2.73E+03		4.87E+03	8.07E+02
C32	Gain of 17.1576	404.3755	12.15							2.89E+03
C33	Gain of 199.3233	586.5412	13.31						2.60E+03	1.49E+03
C34	Gain of 203.2120	590.4299	10.93	3.73E+03	3.66E+03	3.62E+03	5.83E+03		3.99E+03	3.69E+03
C35	Gain of 203.2123	590.4302	10.93	5.70E+03	4.90E+03		6.00E+03		4.47E+03	4.23E+03
C36	Gain of 204.2813	591.4992	13.32			3.04E+03			5.97E+03	4.23E+03
C37	Gain of 21.9590	409.177	9.63					6.34E+03		
C38	Gain of 21.9826	409.2005	6.02						3.47E+03	
C39	Gain of 21.9833	409.2013	6.31		1.32E+03					
C40	Gain of 219.4049	606.6228	12.74		7.04E+03					
C41	Gain of 22.0768	409.2948	11.93				1.25E+03	2.94E+03		
C42	Gain of 22.1113	409.3292	12.15		1.63E+03	2.41E+03			1.90E+03	
C43	Gain of 22.1138	409.3317	12.15		1.91E+03	1.87E+03			1.45E+03	7.02E+02
C44	Gain of 22.1666	409.3845	12.71						5.34E+03	
C45	Gain of 223.3588	610.5768	13.25		4.27E+03					

C46	Gain of 229.5792	616.7972	6.82	1.09E+03	8.82E+02					
C47	Gain of 230.0282	617.2461	6.12	3.39E+04	2.07E+04	2.26E+04	3.22E+04	2.01E+03	1.90E+04	
C48	Gain of 230.0319	617.2498	6.15			8.59E+02				
C49	Gain of 232.3106	619.5285	11.81		7.92E+02	6.94E+02				
C50	Gain of 232.3113	619.5292	11.77	2.06E+03					4.07E+03	3.78E+03
C51	Gain of 247.2385	634.4564	10.93							2.90E+03
C52	Gain of 250.0910	637.309	11.58				3.86E+03			
C53	Gain of 251.3910	638.609	12.43							5.52E+03
C54	Gain of 251.3910	638.6089	12.97	2.39E+03		2.20E+03			3.82E+03	2.29E+03
C55	Gain of 251.3941	638.612	13.47	2.69E+03	2.17E+03				4.30E+03	2.83E+03
C56	Gain of 252.0108	639.2288	6.12	1.09E+03		1.71E+03				
C57	Gain of 255.3856	642.6036	12.72					1.64E+04	1.18E+04	1.12E+04
C58	Gain of 255.3865	642.6044	12.71	8.37E+02						
C59	Gain of 26.0506	413.2685	11.98				4.45E+03			
C60	Gain of 260.3417	647.5596	12.72			8.52E+03				
C61	Gain of 260.3453	647.5632	12.72			2.13E+03	1.83E+03	2.11E+03	1.38E+03	2.24E+03
C62	Gain of 27.1045	414.3224	10.84	5.41E+03	3.79E+03	3.28E+03	3.50E+03		2.64E+03	2.49E+03
C63	Gain of 27.9946	415.2126	9.16					1.74E+03		
C64	Gain of 27.9968	415.2147	9.16				2.93E+03			
C65	Gain of 272.0733	659.2912	11.58		1.52E+03	1.84E+03	1.82E+03		1.04E+03	
C66	Gain of 273.9951	661.2131	6.13	1.34E+04						
C67	Gain of 276.2403	663.4582	13.42						2.53E+03	1.60E+03
C68	Gain of 276.3146	663.5325	12.73		3.69E+03					
C69	Gain of 277.2455	664.4635	10.64	2.25E+03	1.78E+03	1.81E+03				1.61E+03
C70	Gain of 281.4055	668.6234	13.27			5.60E+03				
C71	Gain of 283.9487	671.1666	6.05		9.97E+03	1.07E+04		1.12E+03		
C72	Gain of 283.9504	671.1683	6.13	1.70E+03		1.17E+03				
C73	Gain of 291.2616	678.4796	10.95		1.45E+03	1.76E+03				
C74	Gain of 291.2652	678.4831	10.96					1.18E+05		

C75	Gain of 3.0103	390.2282	6.02					3.41E+03		
C76	Gain of 3.0117	390.2296	6.32	3.00E+03						
C77	Gain of 305.9331	693.1511	6.05	2.42E+03	2.28E+03	1.93E+03			2.51E+03	
C78	Gain of 32.1004	419.3184	12.25				3.28E+03			
C79	Gain of 335.2892	722.5071	10.96						1.59E+03	1.25E+03
C80	Gain of 335.2921	722.51	10.96	1.30E+03					2.55E+03	2.01E+03
C81	Gain of 349.3919	736.6099	13.31					7.24E+03		
C82	Gain of 349.3970	736.6149	13.52				2.12E+03			
C83	Gain of 35.0002	422.2181	8.1				3.86E+03	1.67E+04		
C84	Gain of 352.3926	739.6106	11.85			2.37E+03			2.03E+03	
C85	Gain of 379.3161	766.534	10.96	1.83E+03	2.51E+03	3.08E+03	3.76E+03		2.47E+03	2.17E+03
C86	Gain of 381.4943	768.7122	12.74	3.09E+03	2.31E+03	2.59E+03			4.26E+03	2.76E+03
C87	Gain of 386.2159	773.4339	6.31		2.31E+03	2.34E+03				
C88	Gain of 39.9556	427.1735	8.1					8.09E+03		
C89	Gain of 393.4183	780.6362	13.24							2.12E+03
C90	Gain of 393.4197	780.6377	13.18	6.45E+03	6.55E+03					4.41E+03
C91	Gain of 395.5106	782.7286	13.17	3.08E+03	2.89E+03					
C92	Gain of 4.0688	391.2867	11.98				1.10E+04			
C93	Gain of 40.1767	427.3947	12.81			3.69E+03				
C94	Gain of 407.5107	794.7287	13.19						4.84E+03	3.40E+03
C95	Gain of 408.1972	795.4151	6.31	9.80E+02						
C96	Gain of 409.5274	796.7454	12.82						5.91E+03	
C97	Gain of 423.5439	810.7619	13.49		1.58E+03	2.07E+03				
C98	Gain of 433.5280	820.7459	13.49			2.46E+03				
C99	Gain of 435.5401	822.7581	13.35						3.37E+03	
C100	Gain of 435.5427	822.7607	13.27						3.30E+03	
C101	Gain of 435.5447	822.7626	13.12				8.51E+03			
C102	Gain of 45.0210	432.2389	9.15				6.32E+03			
C103	Gain of 45.0232	432.2412	9.16					4.47E+03	2.74E+03	4.23E+03
C104	Gain of 45.0641	432.282	5.27					2.05E+03		
C105	Gain of 5.8626	393.0806	6.05						2.89E+03	
C106	Gain of 515.6012	902.8192	12.77	2.02E+03		1.66E+03			1.75E+03	1.62E+03

C107	Gain of 54.0823	441.3002	12.23				2.06E+04			
C108	Gain of 57.1144	444.3323	10.52					4.19E+03		9.43E+02
C109	Gain of 6.9801	394.198	6.35		1.50E+03	2.68E+03				
C110	Gain of 6.9822	394.2001	6.4	8.99E+02		1.07E+03				
C111	Gain of 62.0695	449.2875	11.85	8.63E+03	3.44E+04	3.39E+04	4.29E+04	4.04E+04	2.66E+04	1.41E+04
C112	Gain of 62.9944	450.2123	8.52				2.61E+03			
C113	Gain of 63.9471	451.165	8.81					5.57E+03		
C114	Gain of 63.9474	451.1654	9.03					2.05E+03		
C115	Gain of 63.9492	451.1671	8.91					1.30E+03		
C116	Gain of 63.9495	451.1675	8.68					3.70E+03		
C117	Gain of 636.0360	1023.2539	6.03					2.76E+03	1.41E+04	
C118	Gain of 66.1273	453.3452	5.42					4.18E+03		
C119	Gain of 66.1275	453.3455	13.15		3.30E+03					
C120	Gain of 66.1284	453.3464	5.9	4.01E+03					3.29E+03	
C121	Gain of 67.9498	455.1677	8.56		9.44E+02	1.08E+03				
C122	Gain of 67.9503	455.1682	8.94					1.32E+04		
C123	Gain of 68.1193	455.3372	11.75						4.19E+03	
C124	Gain of 71.1307	458.3487	10.86	1.11E+03						
C125	Gain of 72.0871	459.305	12.3	3.00E+03					3.13E+03	3.35E+03
C126	Gain of 76.0856	463.3036	10.86	7.02E+03	5.51E+03	4.78E+03	4.87E+03		3.91E+03	3.90E+03
C127	Gain of 807.6074	1194.8253	13.04			3.44E+03				
C128	Gain of 88.1098	475.3277	5.9	3.04E+03						
C129	Gain of 89.0904	476.3083	5.55		1.27E+04		1.03E+04			
C130	Gain of 90.9904	478.2083	8.94				5.36E+03	1.65E+04		
C131	Gain of 92.2650	479.4829	12.77						4.48E+03	
C132	Hydrogenation	389.2245	6.05						9.29E+02	8.99E+02
C133	Hydrogenation	389.2271	6.27		5.25E+03	4.09E+03	4.47E+03			
C134	Loss of 10.8736	376.3443	11.85	3.09E+03	5.29E+03	1.48E+03	5.71E+03			4.29E+03
C135	Loss of 101.9380	285.2799	11.82		9.55E+02					
C136	Loss of 104.0273	283.1906	9.04					1.93E+03		
C137	Loss of 104.0290	283.189	9.24					8.97E+02		
C138	Loss of 105.0120	282.2059	10.22					7.20E+02		
C139	Loss of 105.0123	282.2056	8.45				2.59E+03			
C140	Loss of 106.1659	281.052	10.25				1.73E+04			
C141	Loss of 107.0292	280.1887	8.89		1.50E+03	1.92E+03				
C142	Loss of 107.0292	280.1888	9.09					7.87E+03		
C143	Loss of 110.1706	277.0474	6.27			1.27E+04				
C144	Loss of 114.9952	272.2227	9.37					5.64E+03		
C145	Loss of 119.0283	268.1896	7.82					8.82E+03		
C146	Loss of 119.0284	268.1895	8.45				3.76E+04			
C147	Loss of 119.0291	268.1888	7.75					3.47E+03		

C148	Loss of 119.0732	268.1448	6.31		2.01E+04	1.52E+04	1.58E+04			
C149	Loss of 119.0738	268.1441	5.99	1.86E+03						
C150	Loss of 119.0738	268.1441	6.06				2.14E+04			
C151	Loss of 119.9486	267.2693	11.84	3.59E+04	9.28E+04	1.15E+05	1.06E+05		1.03E+05	5.79E+04
C152	Loss of 119.9499	267.268	11.83		1.48E+03	1.57E+03			1.21E+03	
C153	Loss of 121.0435	266.1745	8.35				3.48E+04	1.17E+05		
C154	Loss of 121.0444	266.1736	8.56					1.36E+04		
C155	Loss of 121.0449	266.173	8.31					4.89E+03		
C156	Loss of 124.0959	263.1221	6.05		9.26E+02					
C157	Loss of 124.0963	263.1216	6.12	3.02E+03	1.39E+03	1.77E+03				
C158	Loss of 129.0112	258.2067	8.89					3.39E+03		
C159	Loss of 129.0112	258.2068	9.09					7.18E+03		
C160	Loss of 132.1528	255.0651	6.27		4.78E+05	3.93E+05	4.18E+05			
C161	Loss of 133.0059	254.2121	9.37					8.41E+03		
C162	Loss of 135.0220	252.1959	10.4					4.25E+04		
C163	Loss of 137.0391	250.1788	8.45				2.12E+03			
C164	Loss of 138.0606	249.1573	3.84	8.02E+02						
C165	Loss of 14.8687	372.3493	12.22				5.39E+03			
C166	Loss of 14.8694	372.3486	11.79				1.79E+03			
C167	Loss of 14.9728	372.2451	9.65					4.49E+03		
C168	Loss of 140.0738	247.1442	6.53						8.29E+03	
C169	Loss of 140.3547	246.8632	13.73				5.94E+03			
C170	Loss of 143.0271	244.1909	8.31					4.06E+04		
C171	Loss of 145.0060	242.212	9.34					7.80E+03		
C172	Loss of 145.0063	242.2116	8.99					3.17E+03		
C173	Loss of 145.0065	242.2115	9.77	9.40E+02						
C174	Loss of 145.0069	242.211	8.44				1.26E+04			
C175	Loss of 146.1489	241.069	5.35			9.46E+02	6.15E+03		3.55E+03	1.91E+03
C176	Loss of 147.0219	240.196	8.89					1.10E+03		
C177	Loss of 149.0399	238.178	7.88					8.41E+03		
C178	Loss of 15.9004	371.3175	12.03					4.64E+03		
C179	Loss of 151.1043	236.1136	5.35				1.08E+03			

C180	Loss of 153.0557	234.1622	9.59					1.50E+03		
C181	Loss of 154.1027	233.1152	7.03					1.65E+04		
C182	Loss of 154.1031	233.1149	6.7					2.77E+03		
C183	Loss of 155.1234	232.0946	4.33		9.87E+03	7.20E+03	9.37E+02			
C184	Loss of 156.3273	230.8907	13.7				4.78E+03			
C185	Loss of 156.9701	230.2478	10.09					1.01E+03		
C186	Loss of 158.0381	229.1798	9.45	2.96E+03	1.94E+03	2.27E+03	1.46E+03	1.64E+03	2.06E+03	1.78E+03
C187	Loss of 158.1319	229.0861	8.74					7.91E+03		
C188	Loss of 159.0217	228.1962	9.32					1.18E+03		
C189	Loss of 159.0219	228.196	8.41					6.68E+03		
C190	Loss of 159.0223	228.1957	9.99					2.45E+03		
C191	Loss of 159.0428	228.1751	8.48					1.19E+04		
C192	Loss of 16.2364	370.9816	1.17	1.56E+03	1.57E+03	2.05E+03	2.81E+03		3.66E+03	2.64E+03
C193	Loss of 160.0417	227.1763	3.85	9.78E+02						
C194	Loss of 160.0420	227.176	13.32				7.05E+03			
C195	Loss of 160.0516	227.1663	9.11				1.50E+03	5.81E+03		
C196	Loss of 160.2659	226.9521	13.6				4.46E+03			
C197	Loss of 161.0375	226.1804	8.31				9.62E+03	3.79E+04		
C198	Loss of 161.0376	226.1803	9.09					7.27E+03		
C199	Loss of 167.1782	220.0397	13.88				2.10E+04			
C200	Loss of 168.0221	219.1958	9.47					2.52E+03		
C201	Loss of 169.1393	218.0786	4.23		9.77E+02					
C202	Loss of 17.8643	369.3537	12.72			1.11E+04	1.05E+04			
C203	Loss of 17.8655	369.3524	13.03		2.19E+03	1.69E+03				
C204	Loss of 17.8660	369.3519	12.84	2.50E+03						6.14E+03
C205	Loss of 17.8661	369.3518	12.56		1.06E+03					
C206	Loss of 17.8783	369.3396	12.15				1.83E+03			
C207	Loss of 17.9161	369.3019	11.93			1.76E+03			1.55E+03	
C208	Loss of 17.9545	369.2634	10.18					1.52E+03		
C209	Loss of 17.9771	369.2408	11.43	1.79E+04	4.08E+04	4.99E+04	6.44E+04	4.06E+04	3.94E+04	2.47E+04
C210	Loss of 170.1108	217.1072	5.02		1.24E+03					
C211	Loss of 171.0221	216.1958	7.85				3.47E+03	1.14E+04		

C212	Loss of 173.0377	214.1802	7.75					1.81E+04		
C213	Loss of 173.0380	214.18	8.71					1.63E+03		
C214	Loss of 174.2131	213.0048	1.23	6.04E+03	4.22E+03	1.52E+04	1.21E+04	3.37E+03	1.56E+04	6.38E+03
C215	Loss of 174.2132	213.0048	1.44	6.92E+02						
C216	Loss of 176.0485	211.1694	9.24					8.85E+03		
C217	Loss of 176.0487	211.1692	10.02				6.44E+03	1.78E+04		
C218	Loss of 176.0490	211.1689	8.44					2.33E+03		
C219	Loss of 179.0489	208.1691	8.31				2.08E+04	7.87E+04		
C220	Loss of 18.9532	368.2647	8.18					6.23E+03		
C221	Loss of 18.9566	368.2613	11.33							1.02E+03
C222	Loss of 18.9573	368.2606	11.26					1.65E+05		
C223	Loss of 182.1320	205.0859	9.94					2.30E+03		
C224	Loss of 182.1322	205.0857	10.05	1.57E+03				7.55E+03	1.56E+03	1.47E+03
C225	Loss of 182.1495	205.0685	1.14							9.65E+02
C226	Loss of 185.0016	202.2163	6.69	9.79E+02						
C227	Loss of 188.1603	199.0576	3.47	3.94E+03					5.19E+03	2.64E+03
C228	Loss of 19.9341	367.2839	11.64		1.47E+03	1.35E+03				
C229	Loss of 19.9716	367.2463	9.92					2.03E+04		
C230	Loss of 194.0593	193.1586	9.24				3.30E+03	1.18E+04		
C231	Loss of 194.0598	193.1581	8.44				4.29E+03	1.49E+04		
C232	Loss of 195.0585	192.1595	1.41	1.38E+04	8.69E+03	8.98E+03		4.70E+03	2.92E+03	2.29E+03
C233	Loss of 195.1160	192.1019	4.33		2.18E+03	1.57E+03				
C234	Loss of 195.1163	192.1016	5.84		3.14E+03					
C235	Loss of 195.1164	192.1016	4.61		1.31E+03					
C236	Loss of 2.9218	384.2961	8.03					2.58E+03		
C237	Loss of 200.9964	186.2215	6.37					3.25E+03		
C238	Loss of 200.9965	186.2215	5.9	3.70E+03						
C239	Loss of 200.9966	186.2213	6.16							1.13E+03
C240	Loss of 200.9966	186.2213	10.09	1.25E+03				4.78E+03	1.33E+03	1.20E+03
C241	Loss of 201.1266	186.0914	7.44		1.67E+03	1.64E+03				
C242	Loss of 205.0271	182.1909	6.24				1.87E+04			

C243	Loss of 205.0281	182.1898	6.05	1.91E+05	4.20E+05	1.44E+05	1.94E+05	2.56E+04	1.46E+05	2.42E+03
C244	Loss of 209.1320	178.086	4.23	1.47E+04				6.25E+02	4.04E+03	
C245	Loss of 21.9385	365.2795	9.72					1.95E+03		
C246	Loss of 21.9392	365.2787	9.67			1.51E+03			1.69E+03	
C247	Loss of 212.0700	175.1479	9.24					5.86E+03		
C248	Loss of 212.0704	175.1476	8.44					1.05E+04		
C249	Loss of 216.0692	171.1487	6.35	1.29E+03				1.06E+03	1.34E+03	1.09E+03
C250	Loss of 216.1191	171.0988	4.53		1.27E+03					7.75E+02
C251	Loss of 223.1366	164.0813	6.31		4.19E+04	3.26E+04	3.37E+04			
C252	Loss of 223.1367	164.0812	5.99							1.35E+03
C253	Loss of 226.2284	160.9895	1.06						8.92E+02	
C254	Loss of 226.2285	160.9895	13.73				1.32E+04			
C255	Loss of 228.1527	159.0653	5.35	9.11E+02						
C256	Loss of 235.1614	152.0565	1.25		3.12E+03					
C257	Loss of 237.1056	150.1124	1.23			2.62E+03				
C258	Loss of 237.1597	150.0583	1.56	6.81E+02						
C259	Loss of 238.1948	149.0232	10.04				2.83E+03	7.46E+03		
C260	Loss of 238.1950	149.0229	11.97				1.80E+03	2.65E+03		
C261	Loss of 238.1952	149.0228	7.78				5.31E+03			
C262	Loss of 242.2009	145.0171	1.07						5.84E+02	
C263	Loss of 242.2009	145.017	13.7				5.41E+03			
C264	Loss of 245.2594	141.9585	1.07	2.23E+03	2.26E+03	2.75E+03	3.90E+03		4.68E+03	2.43E+03
C265	Loss of 245.2595	141.9584	2.19	5.52E+03	6.48E+03	6.22E+03	6.94E+03	5.82E+03	6.62E+03	6.42E+03
C266	Loss of 25.1784	362.0395	6.14	4.80E+03	4.16E+03	4.95E+03	5.38E+03			
C267	Loss of 251.1425	136.0754	3.92	3.14E+03					9.01E+02	
C268	Loss of 252.1164	135.1015	3.5	4.54E+04	3.06E+04	3.41E+04	1.36E+04		2.00E+04	
C269	Loss of 252.1347	135.0833	4.45	7.76E+02	1.41E+03	8.30E+02			6.93E+02	
C270	Loss of 257.0588	130.1591	4.44					2.63E+03		
C271	Loss of 257.0590	130.1589	4.27	2.03E+03						
C272	Loss of 26.8911	360.3269	12.15	1.69E+03	6.75E+03	6.60E+03	8.21E+03		5.46E+03	2.86E+03

C273	Loss of 26.8929	360.325	12.15					6.21E+03		
C274	Loss of 265.1578	122.0601	3.35	6.39E+03						
C275	Loss of 268.1326	119.0854	7.03	5.00E+03	3.43E+03	3.20E+03			2.64E+03	2.22E+03
C276	Loss of 268.2755	118.9425	13.73				9.80E+03			
C277	Loss of 268.2756	118.9423	1.08						1.65E+03	
C278	Loss of 269.0950	118.123	1.34	1.33E+03						
C279	Loss of 269.0957	118.1223	13.6				2.23E+03			
C280	Loss of 269.1319	118.0861	1.15	3.05E+03	2.70E+03	6.38E+03	6.52E+03		6.76E+03	3.34E+03
C281	Loss of 27.8998	359.3181	11.85	4.72E+03	2.15E+04	2.34E+04	2.87E+04	2.50E+04	1.70E+04	8.82E+03
C282	Loss of 273.1268	114.0911	3.59		2.83E+03	6.60E+03	4.69E+03			
C283	Loss of 28.1122	359.1057	6.77			1.15E+03				
C284	Loss of 282.1846	105.0333	3.35	9.12E+03	6.05E+03	6.29E+03			4.02E+03	
C285	Loss of 285.0900	102.128	1.46	3.57E+03	2.83E+03	2.96E+03			1.86E+03	1.68E+03
C286	Loss of 285.0903	102.1276	1.92	1.18E+03	1.04E+03	9.57E+02			9.65E+02	1.13E+03
C287	Loss of 286.2859	100.932	1.07	1.07E+03	2.84E+03	3.08E+03	5.43E+03		7.19E+03	2.96E+03
C288	Loss of 3.9117	383.3062	11.84		1.66E+03	1.90E+03			1.37E+03	1.00E+03
C289	Loss of 30.9992	356.2188	6.58		2.77E+03					
C290	Loss of 31.9448	355.2731	11.43							1.74E+03
C291	Loss of 32.0082	355.2097	9.04					3.94E+03		
C292	Loss of 32.9318	354.2861	9.64		1.24E+03					
C293	Loss of 33.9492	353.2687	11.43	3.34E+03	1.15E+04	1.26E+04	1.89E+04	1.29E+04	9.39E+03	5.35E+03
C294	Loss of 34.0990	353.1189	5.95	1.65E+04						
C295	Loss of 34.0995	353.1184	6.1	2.01E+03						
C296	Loss of 34.0999	353.1181	4.88	2.26E+03	7.74E+02	3.55E+03	3.33E+03		2.92E+03	1.55E+03
C297	Loss of 34.1013	353.1166	6.09						1.75E+03	
C298	Loss of 34.1272	353.0908	6.12	1.88E+03		2.23E+03				
C299	Loss of 38.2380	348.9799	1.23			7.64E+02				
C300	Loss of 38.9053	348.3127	11.46			1.18E+03				
C301	Loss of 39.0155	348.2024	8.26					4.59E+03		
C302	Loss of 4.0297	383.1882	7.48					5.13E+03		
C303	Loss of 4.0307	383.1872	7.28					2.83E+03		
C304	Loss of 40.1350	347.0829	6.14		1.19E+03					
C305	Loss of 40.9394	346.2785	11.31				9.77E+03			
C306	Loss of 42.9888	344.2292	4.61	1.74E+03	2.40E+03	2.55E+03			2.25E+03	1.87E+03
C307	Loss of 43.9218	343.2961	9.67		1.99E+03	2.02E+03	3.08E+03		1.96E+03	
C308	Loss of 44.0293	343.1886	8.74						2.09E+03	
C309	Loss of 45.9108	341.3072	11.85	1.43E+04	6.29E+04	6.73E+04	8.31E+04	7.31E+04	5.18E+04	2.66E+04
C310	Loss of 45.9120	341.3059	12.73							2.15E+03
C311	Loss of 45.9475	341.2704	11.56			2.65E+03			1.85E+03	

C312	Loss of 48.8756	338.3424	12.15					2.80E+03		
C313	Loss of 5.9173	381.3006	11.84			4.28E+03				
C314	Loss of 5.9194	381.2985	11.84						9.46E+02	
C315	Loss of 5.9206	381.2974	12.21			2.56E+03				
C316	Loss of 5.9546	381.2633	11.56				1.02E+04			
C317	Loss of 50.0942	337.1238	6.77			1.23E+03				
C318	Loss of 50.1415	337.0765	10.25	1.56E+03					1.03E+03	1.08E+03
C319	Loss of 52.0913	335.1267	9.94					4.52E+03		
C320	Loss of 52.1107	335.1073	5					2.99E+03		
C321	Loss of 52.1109	335.107	6.16							9.25E+02
C322	Loss of 54.9217	332.2963	11.8	4.85E+03						5.47E+03
C323	Loss of 54.9379	332.2801	10.14	2.80E+03	3.03E+03				1.46E+03	2.21E+03
C324	Loss of 55.9315	331.2864	11.46	1.04E+03	3.62E+03	4.89E+03	6.80E+03		2.99E+03	1.76E+03
C325	Loss of 58.2120	329.0059	8.76						7.93E+02	1.25E+03
C326	Loss of 58.9500	328.2679	11.31					9.78E+04		
C327	Loss of 60.1385	327.0794	9.62		9.07E+02		8.87E+02	1.02E+03	8.03E+02	9.96E+02
C328	Loss of 60.2092	327.0087	8.76					8.01E+03		
C329	Loss of 60.8385	326.3795	11.84		1.42E+03	1.21E+03				6.59E+02
C330	Loss of 61.9812	325.2367	10.96	2.24E+03	2.41E+03	2.57E+03	4.77E+03		3.30E+03	
C331	Loss of 66.0854	321.1325	5.88				1.77E+04			
C332	Loss of 66.0865	321.1314	6.01					5.96E+03		1.63E+03
C333	Loss of 69.9754	317.2425	1.47	3.16E+03	1.92E+03	2.07E+03	1.36E+03	1.42E+03	1.52E+03	1.54E+03
C334	Loss of 7.9341	379.2838	11.58				5.08E+03			
C335	Loss of 73.9425	313.2754	11.46	4.70E+03	1.66E+04	2.08E+04	2.89E+04	1.93E+04	1.32E+04	7.72E+03
C336	Loss of 77.9900	309.2279	7.15	1.48E+03					1.81E+03	
C337	Loss of 78.0517	309.1663	6.14					1.59E+03		
C338	Loss of 82.9176	304.3003	10.57					4.68E+03		
C339	Loss of 83.0421	304.1759	8.1					2.34E+03		
C340	Loss of 87.9226	299.2954	11.82							6.62E+02
C341	Loss of 88.2442	298.9737	13.58	8.74E+02	8.14E+02	1.19E+03	3.11E+03		1.31E+03	
C342	Loss of 90.0123	297.2056	10.31					5.16E+03		
C343	Loss of 90.0138	297.2041	10.3			1.15E+03				
C344	Loss of 90.1344	297.0835	10.25				3.75E+03			
C345	Loss of 90.9955	296.2224	9.77					4.11E+03		
C346	Loss of 90.9971	296.2208	9.32					4.50E+03		
C347	Loss of 93.0133	294.2046	9.37	1.08E+03						
C348	Loss of 95.1169	292.101	4.7	1.51E+03		2.90E+03	2.67E+03		2.16E+03	1.09E+03
C349	Loss of 95.1173	292.1006	4.55		8.59E+02					
C350	Loss of 98.2946	288.9234	13.63				4.83E+03			
C351	Loss of C16H16N4O+Desaturation	105.0694	5.99	3.25E+05						
C352	Loss of C16H16N4O+Desaturation	105.0696	6.05						1.44E+04	
C353	Loss of C16H16N4O+Desaturation	105.0695	6.31		4.16E+03	4.04E+03	3.73E+03			

C354	Loss of C16H16N4O+Di-Oxidation and Glucuronide Conjugation	315.0942	10.25				1.35E+04			
C355	Loss of C16H16N4O+Glucose Conjugation	269.1274	6.52	1.24E+03					1.08E+03	
C356	Loss of C16H16N4O+Glutamine Conjugation	235.1303	1.27				1.04E+03		6.85E+02	
C357	Loss of C16H16N4O+Glutathione Conjugation and Loss of H2S	380.1926	6.75					1.66E+03		
C358	Loss of C16H16N4O+Hydrogenation	109.101	5.92	3.45E+04					2.89E+04	
C359	Loss of C16H16N4O+Internal Hydrolysis and Di-Oxidation	157.0835	3.5	1.65E+04	8.60E+03	1.12E+04			4.93E+03	
C360	Loss of C16H16N4O+Oxidation and Glutamine Conjugation	251.1279	8.89					3.06E+03		
C361	Loss of C16H16N4O+Oxidation and Sulfate Conjugation	203.0527	1.14					2.79E+03		
C362	Loss of C16H16N4O+Taurine Conjugation	214.0894	7.3					3.30E+03		
C363	Loss of C16H16N4O+Tri-Oxidation and Glucuronide Conjugation	331.1102	6.06						2.37E+03	
C364	Loss of C16H16N4O+Tri-Oxidation and Glucuronide Conjugation	331.1091	6.12			8.35E+02				
C365	Loss of C7H6	297.1713	5.99		1.86E+03					
C366	Loss of C7H6	297.1712	6.05		1.99E+03	1.19E+03				
C367	Loss of C7H6	297.172	6.31		1.07E+03					

C368	Loss of C7H6+Bis-Ketone Formation	325.123	6.62	2.18E+03					2.27E+03	2.60E+03
C369	Loss of C7H6+Di-Hydrogenation	301.2012	9.04					1.61E+03		
C370	Loss of C7H6+Hydrogenation	299.1837	8.99						1.40E+03	2.39E+03
C371	Loss of C7H6+Internal Hydrolysis	315.1781	7.3			1.35E+03			1.06E+03	
C372	Loss of C7H6+Loss of CO	269.1725	8.71					5.40E+03		
C373	Loss of C7H6+Loss of CO	269.173	9.45				4.51E+03	2.17E+04		
C374	Loss of C7H6+Loss of Hydroxymethylene	267.1574	9.11						1.45E+03	1.85E+03
C375	Loss of C7H6+Loss of Hydroxymethylene	267.1573	9.32				7.58E+03	3.13E+04		
C376	Loss of C7H6+Loss of Hydroxymethylene	267.1722	10.25				1.60E+04			
C377	Loss of C7H6+Loss of Water	279.16	10.02				3.54E+03	1.51E+04		
C378	Loss of C7H6+Loss of Water	279.1596	11.97				2.61E+04			
C379	Loss of C7H6+Oxidation	313.1783	9.26				1.09E+03	2.17E+03		
C380	Loss of C7H6+Sulfoxide to Thioether	281.1726	9.59				4.91E+03	1.93E+04		
C381	Loss of C7H6+Sulfoxide to Thioether	281.173	9.87	1.54E+03						1.26E+03
C382	Loss of C8H8	283.1555	5.99	7.93E+02						
C383	Loss of C8H8	283.1553	6.05					8.83E+04	2.91E+05	3.22E+04
C384	Loss of C8H8	283.1563	6.31		1.52E+03					
C385	Loss of C8H8 and C7H6+Demethylation to Carboxylic Acid	223.064	8.96					5.84E+03		

C386	Loss of C8H8 and C7H6+Demethylation to Carboxylic Acid	223.064	10.25				9.27E+03			
C387	Loss of C8H8 and C7H6+Di-Acetylation of Amines	309.1277	4.55					5.07E+03		
C388	Loss of C8H8 and C7H6+Di-Acetylation of Amines	309.1281	4.7	2.14E+03		3.83E+03	3.57E+03		3.04E+03	1.43E+03
C389	Loss of C8H8 and C7H6+Di-Acetylation of Amines	309.1287	6.05		1.06E+03					
C390	Loss of C8H8 and C7H6+Di-Acetylation of Amines	309.128	6.12	7.41E+03	5.99E+03	7.17E+03	6.59E+03		2.00E+03	
C391	Loss of C8H8 and C7H6+Di-Acetylation of Amines	309.1284	6.77	1.48E+03	1.18E+03	4.84E+03			2.48E+03	
C392	Loss of C8H8 and C7H6+Di-Acetylation of Amines	309.1313	8.1					9.86E+03		
C393	Loss of C8H8 and C7H6+Di-Oxidation and Ketone Formation	239.0702	9.94				5.33E+03	1.56E+04		
C394	Loss of C8H8 and C7H6+Hydrogenation	195.1228	2.96	7.20E+02						
C395	Loss of C8H8 and C7H6+Internal Hydrolysis	211.1092	10.25					2.92E+03		
C396	Loss of C8H8 and C7H6+Oxidation and Glucuronide Conjugation	385.1478	6.75			2.54E+03				
C397	Loss of C8H8 and C7H6+Sulfate Conjugation	273.0625	1.23	9.15E+02						
C398	Loss of C8H8 and C7H6+Tetra-Oxidation	257.0848	1.23			1.34E+03			1.33E+03	

C399	Loss of C8H8+Amine to Carboxylic Acid	312.1265	6.12	3.26E+05		3.03E+05	2.56E+05	3.22E+04	1.77E+05	2.67E+03
C400	Loss of C8H8+Demethylation and Di-Oxidation	301.1421	10.04				4.72E+03			
C401	Loss of C8H8+Demethylation and Hydrogenation	271.146	9.19					1.45E+03		
C402	Loss of C8H8+Demethylation to Carboxylic Acid	313.1306	6.13		7.85E+02					
C403	Loss of C8H8+Di-Acetylation of Amines	399.1777	7.63					1.42E+04		
C404	Loss of C8H8+Loss of CO	255.1569	8.05					5.44E+03		
C405	Loss of C8H8+Loss of Hydroxymethylene	253.1447	6.43	1.38E+03		1.33E+03				
C406	Loss of C8H8+Loss of Hydroxymethylene	253.1451	6.62		1.76E+03					
C407	Loss of C8H8+Oxidation	299.1498	5.88	2.10E+03	2.11E+03	2.04E+03	2.12E+03	2.76E+03	2.45E+03	2.33E+03
C408	Oxidation and Internal Hydrolysis	421.2333	10.5					4.84E+03		
C409	Oxidation and Sulfate Conjugation	483.1638	8.94				1.09E+04	5.11E+04		
C410	Oxidation and Sulfate Conjugation	483.1638	9.21					3.02E+03		
C411	Oxidative Deamination to Alcohol	388.1837	6.05		1.79E+03					
C412	Oxidative Deamination to Alcohol	388.1876	6.31		4.72E+03	3.90E+03	3.97E+03			
C413	S-Cysteine Conjugation	506.2038	9.29				4.07E+03	7.21E+03		
C414	Taurine Conjugation	494.2379	8.33				1.44E+04			

Table S3. Plasma metabolites from mice treated with TIC10 were analyzed by mass spectrometry. 8-week old female athymic nude mice treated with TIC10 (100 mg/kg, i.v.). Plasma samples were analyzed by HPLC and fractions were subjected to mass spectrometry analysis. Potential metabolites appearing at later time points are highlighted in light blue. R.T. is the retention time on the HPLC column. Time points refer to time after injection of TIC10.

Peak ID	Name	m/z	R.T. (min)	1 hour	2 hour	2 hour	4 hour	6 hour
C5	Loss of 255.1162	132.1017	1.38					4.31E+04
C6	Loss of 215.1210	172.0969	1.45			5.17E+04		
C7	Loss of 236.1218	151.0961	1.61		1.20E+05			
C8	Loss of 52.0865	335.1315	1.8	2.28E+05				
C9	Loss of 243.1526	144.0653	1.99	3.42E+05				
C10	Loss of 221.1324	166.0856	1.99	2.74E+05	4.03E+05			
C11	Loss of 267.1374	120.0805	2.02		1.42E+05	7.76E+04		1.60E+05
C12	Loss of 201.1054	186.1125	2.14					8.59E+04
C13	Loss of 287.1422	100.0757	2.17	2.85E+05				
C14	Loss of 150.1121	237.1058	2.51	5.11E+05				6.29E+04
C15	Loss of C8H8 and C7H6+Hydrogenation	195.1226	2.61	2.09E+05				
C16	Loss of 170.1131	217.1049	2.61	8.46E+05	1.32E+06	2.98E+05		8.46E+05
C17	Loss of 182.1212	205.0968	2.64		6.32E+05			8.34E+05
C18	Loss of 90.0633	297.1546	3.09		6.21E+04			2.94E+05
C19	Loss of 73.0366	314.1814	3.09	5.08E+05	4.52E+05	3.66E+05		4.10E+05
C20	Loss of 68.0807	319.1372	3.09	1.14E+06	9.48E+05	8.03E+05		
C21	Loss of C8H8	283.1558	3.12	2.53E+05				
C22	Oxidation and Glucuronide Conjugation	579.2464	3.12					1.08E+05
C23	Loss of 270.1276	117.0904	3.18					2.02E+05
C24	Loss of 252.1168	135.1012	3.18					1.17E+06

C25	Loss of 186.1282	201.0897	3.18				6.53E+04	
C26	Loss of 34.0698	353.1482	3.18				7.86E+04	
C27	Loss of 273.1268	114.0912	3.27					1.07E+05
C28	Loss of 285.1268	102.0911	3.38	9.13E+05				1.07E+06
C29	Loss of C8H8 and C7H6+Demethylation and Oxidation	195.0878	3.7					8.51E+04
C30	Loss of 273.1269	114.0911	3.71					6.36E+04
C31	Loss of 104.0426	283.1754	3.84	1.37E+05	2.00E+05			1.89E+05
C32	Loss of 87.0156	300.2024	3.84					8.30E+04
C33	Loss of 82.0604	305.1576	3.84	3.41E+05				
C34	Loss of 208.0904	179.1275	4.01	3.68E+05	5.36E+05			8.07E+05
C35	Loss of 38.0340	349.1839	4.29	6.82E+05	5.57E+04			
C36	Loss of 163.1342	224.0837	4.34	6.23E+05				
C37	Loss of 167.1293	220.0886	4.37	7.65E+05	5.98E+04			
C38	Loss of C8H8 and C7H6+Amine to Carboxylic Acid	222.0857	4.37		4.96E+04			7.53E+04
C39	Loss of 149.1181	238.0999	4.37	3.00E+05	3.58E+04			
C40	Loss of 149.0914	238.1265	4.37		9.32E+05			1.87E+06
C41	Loss of 147.1212	240.0968	4.37		5.89E+04			5.03E+05
C42	Loss of 145.1154	242.1026	4.37					1.78E+05
C43	Loss of 92.0882	295.1297	4.37		2.92E+06			1.78E+07
C44	Loss of C7H6+Oxidation	313.1664	4.45					4.57E+05
C45	Oxidation	403.2139	4.45		1.02E+06			7.45E+06
C46	Demethylation to Carboxylic Acid	417.193	4.45					1.12E+05

C47	Loss of 166.1066	221.1114	4.52	1.08E+06				
C48	Loss of 158.1131	229.1049	4.66				5.11E+04	
C49	Loss of C7H6+Tri-Oxidation	345.1524	4.86				2.32E+05	
C50	Loss of 150.1118	237.1061	5.01				8.08E+04	
C51	Loss of 151.1050	236.1129	5.07				1.80E+06	3.54E+06
C52	Loss of 150.1115	237.1064	5.16					8.16E+04
C53	Loss of C16H16N4O+Desaturation	105.0697	5.26		3.91E+04			
C54	Loss of C8H8	283.1562	5.26	8.01E+04				
C55	Loss of C7H6	297.1719	5.26				5.01E+04	
	Parent	387.2196	5.26	4.47E+05		1.35E+05	6.24E+04	
C56	Loss of C7H6+Bis-Ketone Formation	325.13	5.4	1.77E+05				
C57	Loss of 68.0422	319.1757	5.7	1.01E+06	1.13E+05	6.85E+04	1.82E+05	
C58	Oxidation	403.2138	5.8	4.50E+05	5.09E+04		8.03E+04	
C59	Loss of C8H8+Oxidation	299.1494	5.93	6.36E+06	9.83E+05	6.85E+05	1.63E+06	
C60	Loss of 66.0864	321.1316	5.93	3.89E+04				
C61	Loss of 176.1233	211.0946	6.13		6.30E+04			
C62	Loss of 117.0479	270.17	6.29	4.26E+05				
C63	Loss of 8.0061	379.2119	6.34		9.04E+04			
C64	Ketone Formation	401.1933	6.34		1.16E+05			
C65	Oxidation	403.2132	6.39	3.95E+05				
C66	Loss of 147.1393	240.0786	6.45			4.66E+04		
C67	Loss of C16H16N4O+Glucose Conjugation	269.1361	6.52			4.32E+05	6.62E+04	
C68	Loss of 2.9814	384.2366	6.67			9.01E+04		
C69	Loss of 2.9813	384.2367	6.9	6.39E+04				

C70	Loss of 2.9814	384.2366	7.1		4.80E+04		1.35E+05	
C71	Loss of 150.1121	237.1058	7.15			1.10E+05		
C72	Loss of 154.1026	233.1153	7.17	1.25E+05				
C73	Loss of 268.1328	119.0852	7.21	4.07E+05				
C74	Loss of 197.0953	190.1226	7.27	7.10E+04				
C75	Loss of 202.1009	185.117	7.43		7.06E+04			1.24E+05
C76	Loss of 162.1080	225.1099	7.43	2.02E+05		8.13E+04	7.73E+04	
C77	Loss of 2.9815	384.2364	7.56			4.76E+04	5.24E+04	
C78	Loss of 142.1391	245.0788	7.95		4.16E+04			
C79	Loss of 204.1381	183.0798	8.52	1.39E+05				
C80	Gain of 56.0154	443.2333	8.54	1.54E+05				
C81	Loss of 64.0707	323.1473	8.62	5.50E+04				
C82	Loss of 17.9903	369.2276	8.82		6.02E+05			
C83	Gain of 3.9920	391.2099	8.82	3.14E+05				
C84	Gain of 27.9941	415.2121	9.02	3.14E+05				
C85	Loss of 92.0272	295.1907	9.05			1.01E+05		
C86	Gain of 27.9944	415.2123	9.32		4.82E+04			7.47E+04
C87	Gain of 63.9473	451.1652	9.43		5.52E+04			8.52E+04
C88	Gain of 85.9292	473.1471	9.43			5.43E+04		
C89	Gain of 17.0024	404.2203	9.66			2.42E+05		
C90	Gain of 63.9475	451.1654	9.74		2.87E+05	7.33E+05		1.63E+05
C91	Gain of 85.9292	473.1471	9.74	1.04E+05	6.47E+04	1.72E+05		
C92	Loss of 41.9423	345.2757	9.76			4.59E+04		
C93	Gain of 27.9944	415.2124	9.76		9.58E+04			7.43E+04
C94	Gain of 27.9942	415.2121	9.89	1.99E+05	7.22E+04	3.56E+05		
C95	Gain of 28.0192	415.2372	11.88			1.13E+05		

Table S4. The pharmacokinetics of TIC10 were analyzed in the plasma of C57/B6 mice.

Dose (mg/kg)	t_{max} (h)	C_{max} (μM)	A (h)	B (h)	α (1/h)	β (1/h)	$t_{1/2\alpha}$(h)	$t_{1/2\beta}$ (h)	$AUC_{0-\infty}$ (μM•h)	CL (L/h/kg)	Vd (L/kg)
25	0.02	44.2	44.6	7.67	14.9	0.108	0.047	6.42	63.9	1.01	9.39

Table S5. Overall survival of mice with SF767 intracranial tumors improved with TIC10 and bevacizumab treatment.

Cohort	n	Median Survival (days)	Difference in Median Survival (days)	*P*
Control	8	28	-	-
TIC10	7	74	46	0.038
bev	6	70	42	0.119
TIC10 + bev	7	96.5	68.5	0.0308